# Controlling penguin contributions to CP violation in $B^0 \to J/\psi X$ decays

Universiteit Utrecht, Nikhef

MSc Thesis

Utrecht University

Nikhef


Marten Z. Barel

*Daily supervisor:*

Prof. Dr. Robert Fleischer

Vrije Universiteit Amsterdam

*Project supervisors:*

Dr. Panos Christagoklou

Universiteit Utrecht

Prof. Dr. Raimond Snellings

Universiteit Utrecht


November 3, 2020

# Abstract

Modern particle physics experiments are constantly searching for signs pointing to New Physics (NP) beyond the Standard Model (SM). One possible source for finding NP effects is Charge-Parity (CP) violation in particle-anti-particle mixing of neutral $B_{d(s)}$ mesons. The strength of this CP violation can be parameterised by a weak mixing phase $\phi_{d(s)}$. Accurately measuring the weak mixing phase $\phi_{d(s)}$ and comparing it to SM predictions can provide a signal for NP. Because these mixing phases cannot be directly calculated from Quantum Chromodynamics (QCD), they require experimental input in order to make predictions. It has been known for some time that the results for the mixing phases based on experiments are contaminated by contributions from higher order Feynman diagrams known as penguin diagrams. Controlling these penguin contributions will be necessary in order to improve the precision of these mixing phases in the future. In this thesis the formalism for controlling these penguin contributions is explored. Using the GammaCombo software package a fit is made to the parameters describing these contributions as well as the weak mixing phase $\phi_{d(s)}$. Experimental input in the form of CP asymmetries in $B_s^0 \to J/\psi K_S^0$, $B_d^0 \to J/\psi K_S^0$, $B_d^0 \to J/\psi \pi^0$, $B_s^0 \to J/\psi \phi$ and $B_d^0 \to J/\psi \rho^0$ decays is used for making a global fit to all parameters. This global fit allows for a direct extraction of the mixing phase $\phi_{d(s)}$ from the experimental input and does not require input from QCD calculations. The values for the mixing phases found using this approach agree with currently available measurements. Finally, the signal for NP is explored, as well as how it might change with more accurate experimental input in the future.

# Contents

# Chapter 1

# Introduction

The Standard Model (SM) of particle physics [1] has known a great amount of successes over years, the biggest example of which is probably the discovery of the Higgs boson at the LHC complex in 2012 [2, 3], answering a question that had stood for many years. How do particles get their mass? Another question of similar importance, which as of yet does not have a definitive answer, is why we only observe regular matter in our universe? This question is interesting because when matter is created from pure energy, both matter and antimatter are believed to be created in equal parts. However, some mechanism has lead to an imbalance between matter and antimatter, leaving us only with the former. A possible solution to this problem came to light with the discovery of Charge-Parity (CP) violation in the kaon system by Cronin and Fitch in 1964 [4], providing one of the three conditions for matter-antimatter asymmetry as proposed by Sakharov [5]. In this experiment they observed the decay of a neutral kaon into two charged pions which, at that time, could not be explained via conventional physics, thereby opening the door for CP violating effects. CP violation, simply put, introduces an asymmetry between the decay amplitudes of particles and their antiparticle counterparts. Using this and the fact that matter can oscillate into antimatter and vice versa, it would lead to regular matter becoming the dominant component in the universe over time[1].

In 1974, in order to explain the phenomenon of CP violation, Kobayashi and Maskawa proposed an extension of Cabbibo quark mixing matrix from 1963 [6, 7]. This new matrix, which is now known as the Cabbibo-Kobayashi-Maskawa (CKM) matrix included three generations of quarks and, most importantly, introduced complex coupling constants between quarks. This complex coupling allows for CP violation to occur and, critically, cannot exist with only two generations of quarks. Currently we know for a fact that at least three generations of quarks exist, but at the time that Kobayashi and Maskawa introduced their mixing matrix, only two had been discovered. The presence of this third generation of quarks proposed by Kobayashi and Maskawa was slowly confirmed over time by the discovery of the bottom ($b$) quark in 1977 [8] and the top ($t$) quark in 1995 [9]. Whilst CP violation had already been seen in the second generation of quarks with the observation by Cronin and Fitch, it had yet to be observed in the third at the start of this century. In 2002 these observations were finally made by the Belle and BaBar collaborations at KEK and SLAC respectively by studying the $B^0_d \to J/\psi K^0_S$

[1]The argument can be made that this could in principle happen for either matter or antimatter, but since the distinction between them depends entirely on convention you can always the define the remainder of the two to be "matter" and the other "antimatter"

decay channel [10, 11]. These discoveries confirmed the theory proposed by Kobayashi and Maskawa and rewarded them with the Nobel prize in 2008 [12].

This brings us back to current times. Whilst the SM is a well established theory at this point in time it still faces some problems, the most glaring one possibly being a lack of quantum gravity, although more minor issue also exist. In order to fix these problems many new models of New Physics (NP) have been proposed over the years, but as of yet none of them have been experimentally observed. From this one can draw three conclusions. First, the NP does not exist, which is very hard to prove although at some point a theory can be rejected based on extensive lack of evidence. Second, the effects introduced by the NP do not manifest at the level of energy that is currently achievable with accelerators so in order to confirm the existence of NP, higher energies are required. This is also known as the High Energy frontier. Third, the effects coming from NP are very small and as of yet fall within the margin of error of experimental observations, so in order to observe NP, higher accuracy is required. This is known as the High Precision frontier.

It is this High Precision frontier that is being explored in Flavour Physics, which concerns itself with the mechanisms behind quark and lepton flavour mixing within the SM, in which the CKM matrix plays a major role. As it stands now, the CKM matrix provides a good description of the mechanism for CP violation and flavour mixing, it is however entirely possible for NP effects to enter in these processes. If this is the case, accurate measurements of the CKM matrix parameters should show tensions with SM predictions and lead to evidence of NP effects. One of these searches for NP is the measurement of the weak mixing phases $\phi_s$ and $\phi_d$ which parameterise the strength of CP violation in $B^0_{s(d)} - \bar{B}^0_{s(d)}$ mixing. The SM provides a description for this mixing process via the CKM quark mixing matrix but it is possible for NP to mediate the process and introduce a phase shift to the weak mixing phases. Therefore, by accurately measuring these phases it might be possible to detect these NP effects and give an estimation for the size of their contribution. The weak mixing phases mentioned above can be studied through neutral B meson decays, which are sensitive to CP violation in $B^0_{s(d)} - \bar{B}^0_{s(d)}$ mixing. The mixing phases $\phi_s$ and $\phi_d$ can in general be expressed as:

$$\phi_q = \phi_q^{\mathrm{SM}} + \phi_q^{\mathrm{NP}}, \tag{1.1}$$

with $q \in (d, s)$. In order to accurately measure the SM phase and the NP contribution it is important to know what processes contribute to the decay being studied. As with most phenomena in high energy (particle) physics, these processes can be split into orders, with each subsequent order contributing less to the overall process. For any sort of particle interaction or decay, these processes are described by making use of Feynman diagrams, which provide both a visual interpretation of the interaction, as well as a mathematical blueprint with which the interaction rate can be calculated. For the neutral $B$ decays that will be studied in this thesis, the leading order contribution to these decays are called tree diagrams, with the next-to-leading order being made up of penguin diagrams. The former being named such because the diagram somewhat resembles a tree, the latter got its name from John Ellis after losing a bar-room bet in 1977 [13]. Whilst the tree diagrams entering these decays have long been understood and described, a formalism for estimating the contributions coming from the penguin diagrams was first proposed by Robert Fleischer in 1999 [14, 15]. In these papers he discussed a method for extracting CKM angles from $B \to J/\Psi X$ decays. This formalism was then expanded upon in

2008 [16] in order to correct for the contribution of penguin diagrams to the B meson mixing phases. So far the penguin parameters were determined in $B_d^0$ decays, but in 2010 [17] they were also determined from observations of CP violation in $B_s^0 \to J/\psi K_S^0$. Finally a roadmap for controlling the penguin contributions via several decay channels was presented in 2015 by Kristof de Bruyn and Robert Fleischer [18]. It is this last paper which forms the basis for the research done in this thesis.

Since the publication of the 2015 paper new results for CP violation parameters in neutral $B$ decays have become available and more results coming from the finished run 2 at LHC are expected soon. The completion of the Belle II detector at the SuperKEK facility should also provide exciting new results for Flavour Physics. In light of this it is useful to see what has changed since 2015 and give an update on the penguin parameters entering the neutral $B$ decays.

The goals for this thesis are to determine the size of the penguin parameters in neutral $B$ decays; To find the size of the penguin corrections to the weak mixing phases $\phi_d$ and $\phi_s$; And to obtain clean measurements of $\phi_d$ and $\phi_s$. To aid further research on this topic as well as inclusion of the penguin corrections into the global CKM parameter search, a fitting module is developed within the GammaCombo software package from LHCb [19].

The outline of this thesis is as follows. In Chapter 2, I will explore the theoretical background to discuss these penguin contributions, starting with a general introduction of the SM and a more thorough explanation of the Feynman diagrams mentioned above. This is followed by a discussion of the field of Flavour Physics and CP violation from which we get the basic tools needed to measure the mixing phases. Finally, the formalism for controlling the penguin contributions as put forward in previous papers is explored in detail. In Chapter 3, I will discuss the GammaCombo fitting module in more detail, followed by an overview of the decay channels that are used to measure the penguin contributions to $\phi_d$ and $\phi_s$. In Chapter 4, I will show the results of the fit to the penguin parameters as well as a more detailed look at the interplay between the decay channels that are used. Finally in Chapter 5, I will discuss these results and the analysis as a whole and see what conclusions can be drawn from them, as well as an outlook for how these results might be improved in the future.

# Chapter 2

# Theoretical framework

## 2.1 Background information

Before I outline the formalism that is used for answering the questions asked in the introduction it is useful to known the surroundings in which this formalism is placed. To that end I will start with introducing background information which is needed to properly understand the formalism for describing the penguin contributions.

### 2.1.1 The Standard Model of particle physics

Almost all research into particle physics that is done currently involves the Standard Model (SM) in some capacity. In general terms, the Standard Model provides a description of the most fundamental particles in nature and the forces that act on these particles. More specifically, the SM is a quantum field theory build up out of gauge symmetries. These symmetries are

$$SU(3)_{colour} \times SU(2)_{I_3} \times U(1)_Y, \tag{2.1}$$

where *colour* is colour charge, $I_3$ is weak isospin and $Y$ is hypercharge. This is complemented by spontaneous symmetry breaking of the $SU(2)_{I_3} \times U(1)_Y$ symmetries via the Higgs mechanism [20, 21, 22], allowing the associated gauge bosons to have mass and introducing an additional massive gauge boson, now known as the Higgs boson, in the process.

These three symmetries describe all possible interactions that can occur between the particles that make up the SM. All such interactions are mediated by gauge bosons, which are generated by the symmetry groups listed above. In general any interaction between particles can either transfer charge from one particle to the other, these are called charged current (CC) interactions, or transfer no charge, called neutral current (NC) interactions. Any charge that is transferred via these interactions has to be carried by the mediating boson.

$SU(3)_{colour}$ describes the strong interactions between quarks. These interactions are NC interactions mediated by a set of 8 gluons ($g$), each carrying a different colour charge. This colour charge provides the basis for how quarks form bound states. The bound states are required to have no net colour, or in other words, they must be white. A quark can carry either a red, blue or green colour charge, which can be interchanged via strong interactions, where the colour being transferred is carried by the mediating gluon.

| | Charge (e) | Spin (J) | Mass |
|---|---|---|---|
| $\gamma$ | 0 | 1 | 0 |
| $g$ | 0 | 1 | 0 |
| $Z^0$ | 0 | 1 | $91.1867 \pm 0.0021$ GeV |
| $W^{\pm}$ | $\pm 1$ | 1 | $80.379 \pm 0.012$ GeV |

Table 2.1: Basic properties of gauge bosons.[23]

| Name | Charge (e) | Spin ($I_3$) | Mass (MeV) |
|---|---|---|---|
| up ($u$) | 2/3 | +1/2 | $2.16^{+0.49}_{-0.26}$ |
| down ($d$) | -1/3 | -1/2 | $4.67^{+0.48}_{-0.17}$ |
| charm ($c$) | 2/3 | 0 | $(1.27 \pm 0.02) \times 10^3$ |
| strange ($s$) | -1/3 | 0 | $92^{+11}_{-5}$ |
| top ($t$) | 2/3 | 0 | $(172.76 \pm 0.3) \times 10^3$ |
| bottom ($b$) | -1/3 | 0 | $(4.18^{+0.03}_{-0.02}) \times 10^3$ |

Table 2.2: Basic properties of quarks. [23]

$SU(2)_{I_3} \times U(1)_Y$ together describe both the electromagnetic and weak interactions between particles. The electromagnetic interactions are NC interactions between charged particles and are mediated by the photon ($\gamma$). The weak interactions between particles are either CC interactions mediated by the $W^+$ and $W^-$ bosons, or NC interactions mediated by the $Z^0$ boson. The properties of the gauge bosons are listed in Table 2.1.

Besides the gauge bosons the SM also contains the fundamental particles between which the interactions can occur. These particles can be divided into two sectors, the quark sector and the lepton sector. The quark sector contains 6 particles that can be divided into three generations. An overview of these particles and some of their properties is given in Table 2.2. Each generation of quarks forms a doublet with one up type and one down type quark. The first generation consists of the up and the down quark, the second generation consists of the charm and strange quark, and the third generation consists of the top and bottom quark. They are the only particles that can interact with each other via the strong force and because of this are always found in bound colour-neutral states in nature.

Similar to the quark sector, the lepton sector can also be divided into three generations, each consisting of a doublet made up of a lepton, and the associated lepton-neutrino. As with the quarks, also here the first generation features the lightest particles, and the third generation the heaviest ones. The leptons carry unit charge and can not interact via the strong force. Because of this they are found freely in nature. The neutrinos that accompany the leptons in each generation carry no charge and as such only interact via the weak force.

Another class of particles that is of importance but not directly a part of the SM is that of hadrons. Hadrons are bound states of quarks with each hadron consisting of either two or three quarks. Since hadrons do not carry colour only combinations of three quarks, called baryons, or of quark anti-quark pairs, called mesons, are possible. The most common examples of baryons are the proton and the neutron, which make up all nuclear matter found in nature. The first meson that was observed experimentally is the pion ($\pi$) which is made out of up and down quarks. A list of mesons that will

| Name | Content | Mass (MeV) | $J^{PC}$ |
|---|---|---|---|
| $\pi^0$ | $\frac{1}{\sqrt{2}}(u\bar{u}+d\bar{d})$ | $134.9768 \pm 0.0005$ | $0^{-+}$ |
| $K^0$ | $u\bar{s}$ | $497.611 \pm 0.013$ | $0^-$ |
| $J/\psi$ | $c\bar{c}$ | $3096.900 \pm 0.006$ | $1^{--}$ |
| $B_d^0$ | $d\bar{b}$ | $5279.65 \pm 0.12$ | $0^-$ |
| $B_s^0$ | $s\bar{b}$ | $5366.88 \pm 0.14$ | $0^-$ |
| $\rho^0$ | $u\bar{u}$ | $775.26 \pm 0.25$ | $1^{--}$ |
| $\phi$ | $s\bar{s}$ | $1019.461 \pm 0.016$ | $1^{--}$ |

Table 2.3: Basic properties of mesons encountered in this thesis. Listed are the quark content, mass and the J, C and P quantum numbers. The charge has been omitted since all of these particles are neutral. For $K^0$, $B_d^0$ and $B_s^0$ only the P number is known. For the B mesons this is a predicted value. These three particles do not have a quantum number C due to them not being C eigenstates. [23]

feature heavily in this thesis is given in Table 2.3. We can make yet another classification of hadrons based on their angular momentum J. This mostly pertains to the way the particle acts under the C, P and T transformations in the Hamiltonian. Particles with J = 0 act like scalars, whilst particles with J = 1 act like vectors. For completeness sake, if a particle has J = 2, it acts like a tensor, the only particle that is currently thought to have J = 2 is the graviton, which is the gauge boson associated with quantum gravity. Under this classification we can make a further division based on the P eigenvalue of the particles. For the case J = 0, if P = +1, we get a "proper" scalar states, if P = -1 we get a pseudo-scalar state. For the case J = 1, with P = -1 we get vector states, with P = +1 we get axial vector states. Looking at Table 2.3, $\pi$, $K^0$ and the $B$ mesons are pseudo-scalar states and $J/\psi$, $\rho$ and $\phi$ are vector states. The Particle Data Group [24] keeps track of all currently known hadrons and SM particles, as well as current searches for new particles and physics.

### 2.1.2 Feynman Diagrams

Now that we have seen the particles and forces described by the SM, I can start explaining the interactions these particles can have and how these are described. In modern physics, any interaction between particles is typically described by using Feynman diagrams, of which a simple example can be seen in Fig. 2.1. A Feynman diagram is built up of external lines, internal lines and vertices where these lines connect. An external line is one that represents the particles entering or exiting the interaction. The internal lines represent all particles involved in the interaction which are not observed after the fact. The internal lines typically include the mediating gauge bosons and possibly quarks and/or leptons running in loops. Whilst at face value this is a very intuitive system to use it follows a set of strictly defined rules that dictate what each line represents. Using these rules to read a diagram yields the formula necessary for calculating the transition amplitude of the interaction shown in the diagram. One of the great strengths of the Feynman diagrams is that it allows one to come up with new interactions that might not yet have been observed, and consequently make predictions which can be tested with experiments.

When a particle decays, it can decay in to any state for which a Feynman diagram can be constructed following the Feynman rules. It is possible for a single decay to be allowed

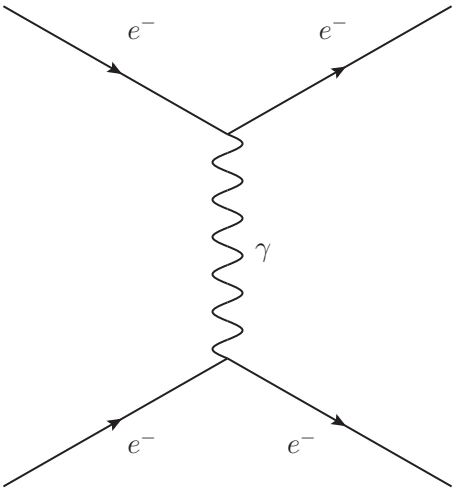


Figure 2.1: Simple Feynman diagram of $e - e$ scattering.

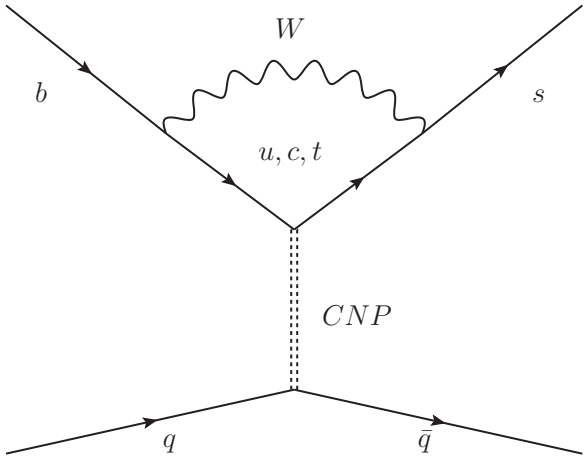


Figure 2.2: Generic penguin diagram featuring a $b \to s$ transition. $CNP$ is a colour neutral propagator which can be a $g$, $\gamma$ or $Z^0$ boson.

via multiple Feynman diagrams, in which case the total transition amplitude is given by the superposition of all possible Feynman diagrams. In any decay it is always possible to construct additional Feynman diagrams describing the decay by introducing particle loops. Adding such a loop to the diagram lowers the transition amplitude compared to the diagram without a loop. Because of this, all Feynman diagrams transcribing a decay can be ordered by their transition amplitudes. The leading order diagrams typically do not feature any loops, with each subsequent order adding one more loop to the diagram. In order to get a reasonable estimate for the total transition amplitude of any given decay it is usually sufficient to only study the leading order diagrams. However, when more accuracy is needed, next-to-leading order diagrams should be taken into account.

For the neutral B decays that are studied in this thesis the leading order diagrams are called "tree" diagrams and as such the leading order is often times referred to as tree-level. The next order of diagrams which describe the neutral B decays are the so-called "penguin" diagrams. The penguin diagrams have distinct shape (which can be drawn to resemble a penguin) and were named such by John Ellis in 1976 after losing a bet over a

game of darts [13], the structure of a generic penguin diagram is shown in Fig. 2.2.

## 2.2 Flavour Physics

Research into the SM can be divided further into fields. One such field is flavour physics, that studies quark flavours, which indicates the quark type, and the properties that these flavours have. Interactions between quarks can be mediated by every force in the SM, but only the weak force couples to the flavour of quarks, rather than just electric charge or colour. A major part of flavour physics is the study of CP violation.

### 2.2.1 CP violation

As mentioned in the introduction the primary motivation for this thesis is research into the properties of CP violation and the possibility of measuring NP. As we have seen with the SM above, most of modern physics is based upon symmetries. In the case of interactions as described by Feynman diagrams there are some further symmetries of these interactions that are important besides the symmetry groups from which the SM is constructed. These include symmetry under charge conjugation (C), Parity-inversion (P) and Time reversal (T). In any interaction the product of C, P and T has to be conserved. For a while it was thought that each of these symmetries had to be conserved individually, but this turned out not to be the case.

The reason for this has to do with the chirality of particles. The chirality of a particle can also be referred to as the handedness of a particle, with them being either left or right handed. A similar concept to this is that of helicity, which describes the size of the particles spin along it's direction of movement. For massless particles the chirality and the helicity of the particle is the same. However, for particles with mass this is no longer the case, since a frame of reference can be chosen such that its helicity is reversed compared to the helicity in the lab frame.

In order to describe the C and P symmetry operations, let $\Psi_L$ be a left handed particle with momentum $\vec{p}$. If we now apply C we get:

$$C|\Psi_L(\vec{p})\rangle = \eta_\Psi^C|\bar{\Psi}_L(\vec{p})\rangle, \tag{2.2}$$

here $\eta_\Psi^C$ is the eigenvalue of the transformation under C and equals $\pm 1$. Note that the chirality of the particle did not change, but C did make a conversion to an antiparticle. When applying the P transformation we get

$$P|\Psi_L(\vec{p})\rangle = \eta_\Psi^P|\Psi_R(-\vec{p})\rangle, \tag{2.3}$$

where $\eta_\Psi^P$ once again describes the eigenvalue of the particle under P. Note however that this time the P transformation changed the handedness of the particle involved. The reason why C and P (and as it happens, CP) are not conserved in nature is because of the weak interaction. The weak interaction only acts on left-handed particles, or right-handed antiparticles. Using this, it is quite easy to see why C and P are not individually conserved under weak interactions, since effectively they both change the handedness of the particle. For P this is quite obvious and whilst C might not seem to change the handedness outright, it happens that the chirality of a particle and its antiparticle is also

reversed. So a right-handed antiparticle interacts under the weak interaction as if it is a left-handed particle. The solution to this problem seems quite obvious. By applying both the C and P transformation to a particle, it's handedness should be conserved. Using the same descriptions as before we get

$$CP|\Psi_L(\vec{p})\rangle = \eta_\Psi^{CP}|\bar{\Psi}_R(-\vec{p})\rangle, \tag{2.4}$$

where $\eta^{CP}$ describes the eigenvalue of the particle under CP and simply equals $\eta^C \cdot \eta^P$. As we can see, the left handed particle has now been transformed into a right handed antiparticle.

It turns out however, that there are decays in which CP is not conserved. The first example, which in turn led to the discovery of this concept, is the decay of $K^0$. When observed in nature this particle turns out to have two different states, one with a short lifetime, $K_S^0$, and one with a longer lifetime, $K_L^0$. At first glance, these two states are CP eigenstates, this means that under CP transformation the state changes up to a difference in sign. The difference between the two is that $K_S^0$ is a CP even state, whereas $K_L^0$ is CP odd, in other words, the CP-eigenvalue of $K_S^0$ is $\eta_{CP} = +1$ and the eigenvalue of $K_L^0$ is $\eta_{CP} = -1$. Assuming that CP is conserved in weak decays, the CP eigenvalue of the initial state and final state particles must be the same. So $K_S^0$ is only allowed to decay into CP-even final states. As it turns out, this is not the case. in 1964 it was discovered that the CP-even $K_S^0$ could decay into a CP-odd final state! In other words, CP was violated.

In general there are three types of CP violation that can be observed. The first type is mixing induced CP violation. It occurs when the rate $A(\Psi \to \bar{\Psi}) \neq A(\bar{\Psi} \to \Psi)$, and as such is time dependent. The second type is direct CP violation. In this case the rate $A(\Psi \to f) \neq A(\bar{\Psi} \to \bar{f})$. Finally there is also the possibility for both of these types of CP violation to manifest in one decay. In these cases, the initial state particle or antiparticle both decay to a final state which is a CP eigenstate, so $f = \bar{f}$. In these cases CP violation can occur directly, when $A(\Psi \to f) \neq A(\bar{\Psi} \to f)$, or indirectly when $A(\Psi \to \bar{\Psi}) \neq A(\bar{\Psi} \to \Psi)$. A combination of both when $A(\Psi \rightsquigarrow \bar{\Psi} \to f) \neq A(\bar{\Psi} \rightsquigarrow \Psi \to f)$. In any of these cases, $\Psi - \bar{\Psi}$ mixing induces interference effects in CP violation, leading again to a time dependence.

For the neutral kaon system in which CP violation was first observed, $K^0 - \bar{K}^0$ mixing had the largest contribution, although some direct CP violation also occurred. The strength of the mixing induced CP violation in kaons is described by the parameter $\epsilon$, for direct CP violation the parameter $\epsilon'$ is used. $\epsilon$ itself is relatively small at $\mathcal{O}(10^{-3})$, but $\epsilon'$ is even smaller with $\epsilon'/\epsilon \approx 10^{-3}$ [23].

### 2.2.2 CKM Matrix and Unitarity Triangles

In order to allow for CP violation in the SM, it is necessary to describe how weak decays occur and in particular, how changing from a particle to an antiparticle results in different transition rates. As mentioned in the introduction, the concept of quark mixing already existed before the discovery of CP violation. However, Cabibbo's 2x2 matrix can not allow for a description of CP violation. In order for it to occur through quark mixing there needs to be a complex phase that can enter the transition amplitudes. To allow for this phase, Kobayashi and Maskawa proposed an extension of Cabibbo's quark mixing matrix to include three generations of quarks. This matrix is now commonly referred to

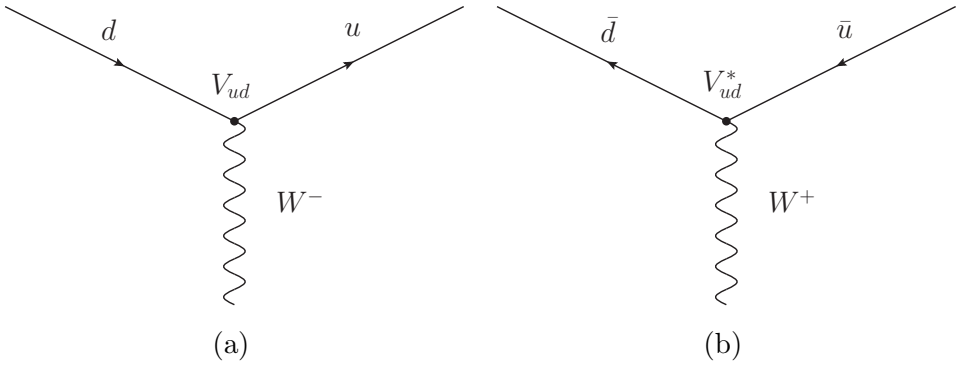


Figure 2.3: Feynman diagrams of (a) a $d \to u$ transition and (b) a $\bar{d} \to \bar{u}$ transition with W emission. The corresponding CKM elements are listed as well.

as the Cabibbo-Kobayashi-Maskawa (CKM) matrix. Besides allowing for a description of CP violation in the SM the CKM matrix also allows for a clean description of the Yukawa couplings through which the quarks gain their mass. Through this definition, the CKM matrix describes how the interaction eigenstates of quarks mix into the (Yukawa) mass eigenstates. When defining the matrix this way one can choose to let either the up-type quark or the down-type quark interaction eigenstates be equal to the mass eigenstates. Convention dictates that the up-type quarks remain unchanged, and as such we have for the down type interaction eigenstates:

$$\begin{pmatrix} d \\ s \\ b \end{pmatrix} = \begin{pmatrix} V_{ud} & V_{us} & V_{ub} \\ V_{cd} & V_{cs} & V_{cb} \\ V_{td} & V_{ts} & V_{tb} \end{pmatrix} \begin{pmatrix} d' \\ s' \\ b' \end{pmatrix} . \tag{2.5}$$

Here the primed quarks correspond to the mass eigenstates, and the unprimed quarks to the interaction eigenstates. The matrix elements $V_{ij}$ are known as CKM elements. Through diagonalising the Yukawa couplings the CKM matrix enters in charged-current (CC) interactions between quarks. As such, each CKM element describes how strongly one quark flavour couples to another under weak interactions. For example, when a $d$ quark decays into an $u$ quark whilst emitting a $W^-$ boson, the strength of the coupling is given by $V_{ud}$. The Feynman diagram of this transition as well as its CP counterpart is shown in Fig. 2.3. Since charge is carried in these interactions though the mediating charged W bosons, it is not possible for an up type quark to decay or change flavour directly into another differently flavoured up type quark, the same holds for down type quarks. In other words, there are no flavour changing neutral current (FCNC) interactions at tree level within the SM. It is however possible to construct next-to-leading order diagrams in which a down type quark ends up decaying into a differently flavoured down type quark. An example of such a diagram is the penguin diagram shown in Fig. 2.2 where a $b$ quarks decays into an $s$ quark. The diagrams that feature a FCNC always involve quarks running in a loop together with a W boson, effectively combining two CC interactions to form a FCNC interaction. As such FCNCs will always involve at least 2 CKM elements.

The CKM elements can be parameterised in a few different ways. One standard choice

is the following:

$$V_{CKM} = \begin{pmatrix} c_{12}c_{13} & s_{12}c_{13} & s_{13}e^{-i\delta} \\ -s_{12}c_{23} - c_{12}s_{23}s_{13}e^{i\delta} & c_{12}c_{23} - s_{12}s_{23}s_{13}e^{i\delta} & s_{23}c_{13} \\ s_{12}s_{23} - c_{12}c_{23}s_{13}e^{i\delta} & -c_{12}s_{23} - s_{12}c_{23}s_{13}e^{i\delta} & c_{23}c_{13} \end{pmatrix}, \tag{2.6}$$

where $s_{ij} = \sin\theta_{ij}$ and $c_{ij} = \cos\theta_{ij}$. $\delta$ is the complex phase that allows for CP-violation. The angles $\theta_{ij}$ can be chosen such that $s_{ij}$ and $c_{ij}$ become positive. Whilst these parameters allow for a completely analytical description of the CKM matrix, it is quite cumbersome to work with. Instead I will be using the Wolfenstein parameterization by defining [25, 26]

$$s_{12} = \lambda, \quad s_{23} = A\lambda^2, \quad s_{13}e^{i\delta} = A\lambda^3(\rho + i\eta). \tag{2.7}$$

Where $\lambda \approx |V_{us}| \approx 0.22$. Since $s_{13}$ and $s_{23}$ are quite small ($O(10^{-3})$ and $O(10^{-2})$) we can set $c_{13} = c_{23} = 1$ with good accuracy. If we then apply (2.7) the CKM matrix takes the following form:

$$V_{CKM} = \begin{pmatrix} 1 - \frac{\lambda^2}{2} & \lambda & A\lambda^3(\rho - i\eta) \\ -\lambda & 1 - \frac{\lambda^2}{2} & A\lambda^2 \\ A\lambda^3(1 - \rho - i\eta) & -A\lambda^2 & 1 \end{pmatrix} + O(\lambda^4). \tag{2.8}$$

In order to diagonalise the Yukawa mass matrices the CKM matrix is required to be unitary. A matrix $U$ is defined to be unitary if the following equation holds:

$$U^\dagger U = \mathbb{1} \tag{2.9}$$

Applying this to the CKM matrix yields equations with the following form:

$$V_{ui}V_{uj}^* + V_{ci}V_{cj}^* + V_{ti}V_{tj}^* = 0 \tag{2.10}$$

or, when we take $UU^\dagger = \mathbb{1}$,

$$V_{kd}V_{ld}^* + V_{ks}V_{ls}^* + V_{kb}V_{lb}^* = 0. \tag{2.11}$$

Where $i \neq j \in (d, s, b)$ and $k \neq l \in (u, c, t)$. In total there are 12 of these equations, half of which are simply complex conjugate forms of the other half, effectively leaving us with 6 equations. From the diagonal we get

$$V_{id}V_{id}^* + V_{is}V_{is}^* + V_{ib}V_{ib}^* = 1, \tag{2.12}$$

with $i \in (u, c, t)$.

Looking again at the Wolfenstein parameterisation we can see that there exists a certain hierarchy to the CKM elements, by order of lambda. The mixing between quarks is largest within one generation, being about order 1. Second largest is the mixing between first and second generation quarks with order $\lambda$. The elements that describe mixing between the second and third generation are about order $\lambda^2$, and the smallest are the elements describing mixing between the first and third generation, at order $\lambda^3$. If we now look back at the equations listed above we can make some interesting observations. Since all of the quantities involved are complex numbers we can plot them in the complex plane. When doing so we can see that they form triangles, also known as unitarity

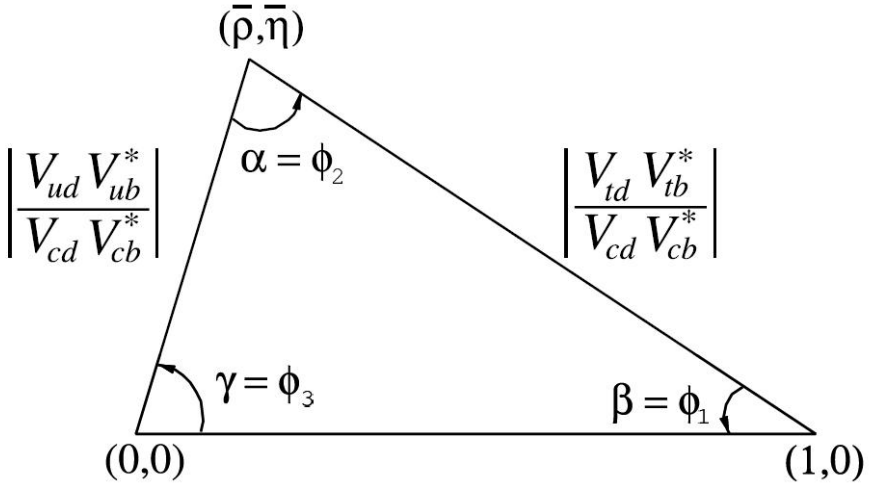


Figure 2.4: The unitarity triangle given by (2.14). This triangle also includes NLO terms by setting $\bar{\rho} = \rho(1 - \lambda^2/2)$ and $\bar{\eta} = \eta(1 - \lambda^2/2)$ [27].

triangles (UTs). If one writes out the equations listed above we can see that there are two equations where each of the three terms are of order $A\lambda^3$. One of the triangles is given by

$$V_{ud}V_{ub}^* + V_{cd}V_{cb}^* + V_{td}V_{tb}^* = 0. \tag{2.13}$$

We can normalise the bottom side of the triangle by diving out $V_{cd}V_{cb}^*$ and getting

$$1 + \frac{V_{ud}V_{ub}^*}{V_{cd}V_{cb}^*} + \frac{V_{td}V_{tb}^*}{V_{cd}V_{cb}^*} = 0. \tag{2.14}$$

The sides can be parameterised by setting

$$\frac{V_{ud}V_{ub}^*}{|V_{cd}V_{cb}^*|} \equiv R_b e^{i\gamma} \quad \text{and} \quad \frac{V_{td}V_{tb}^*}{|V_{cd}V_{cb}^*|} \equiv R_t e^{i\beta}. \tag{2.15}$$

Where

$$R_b = \left|\frac{V_{ud}V_{ub}^*}{V_{cd}V_{cb}^*}\right|, \quad R_t = \left|\frac{V_{td}V_{tb}^*}{V_{cd}V_{cb}^*}\right|, \tag{2.16}$$

and

$$\gamma = \arg\left(-\frac{V_{ud}V_{ub}^*}{|V_{cd}V_{cb}^*|}\right), \quad \beta = \arg\left(\frac{V_{td}V_{tb}^*}{|V_{cd}V_{cb}^*|}\right) \tag{2.17}$$

This UT is also shown in Fig. 2.4. Another triangle, which is more relevant to the neutral B decays, is given by

$$V_{us}V_{ub}^* + V_{cs}V_{cb}^* + V_{ts}V_{tb}^* = 0. \tag{2.18}$$

In this triangle two of the sides are of order $A\lambda^2$, with one side being much smaller at order $A\lambda^4$. As such the triangle appears to be squashed compared to the one given by (2.14). These kinds of relations are however quite useful for doing calculations since they provide relations between the different CKM elements. This is especially true when considering Feynman diagrams featuring quark loops. The triangle above could be used in decays featuring a $b \to s$ transition. Since this process is a FCNC it can not occur at tree level and loops have to be used to construct the diagram. Since any up type quark can enter

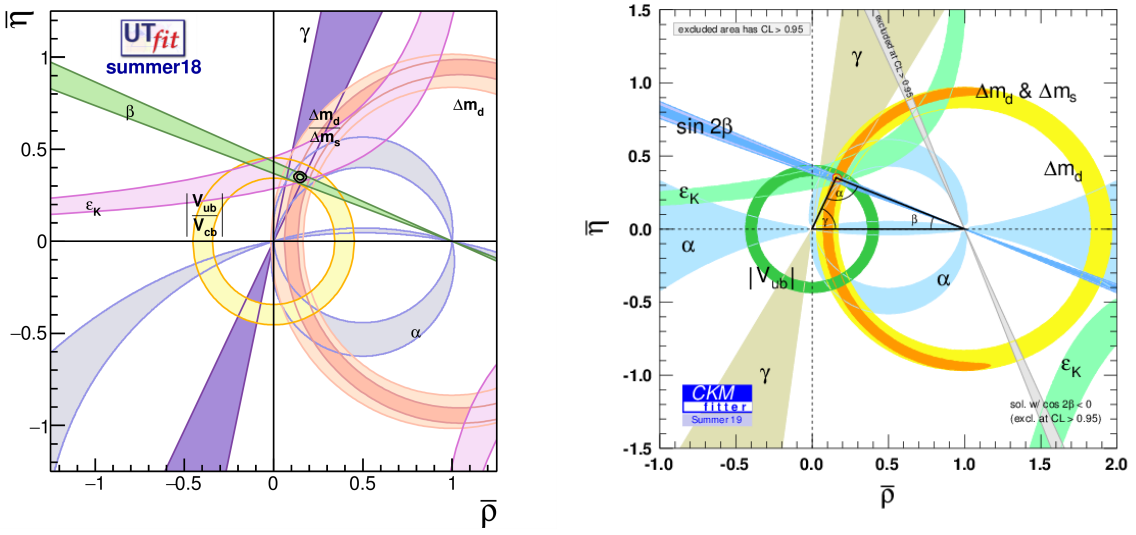


(a) (b)

Figure 2.5: Current fit of the standard unitarity triangle by the UTfit collaboration (a) and the CKMfitter collaboration (b) in the $\bar{\rho} - \bar{\eta}$ plane. The region being fitted for in both is the apex of the triangle given by $(\bar{\rho}, \bar{\eta})$.

this loop the relation above is very useful for reducing the amount of CKM elements entering the full transition amplitude. These unitarity triangles are still actively being researched since they can provide crucial insights into the mechanism of CP violation and possible NP effects. Nowadays there are two groups that are researching the UTs, these are the CKMfitter collaboration [28] and the UTfit collaboration [29]. Research into the UTs involve a variety of decay channels including semileptonic $B$ decays, $K - \bar{K}$ mixing and $b$ hadron decays. The fits that are made by these two collaborations can be seen in Fig. 2.5.

### 2.2.3 Operator Product Expansion

Another useful tool in the toolbox for flavour physics is Operator Product Expansion (OPE). Let us begin by considering a $c \to s u \bar{d}$ transition, mediated by a W exchange. Ignoring possible contributions from strong (QCD) interactions for the moment, the transition amplitude for this process is given by [30]

$$A = -\frac{G_F}{\sqrt{2}} V_{cs}^* V_{ud} \frac{M_W^2}{k^2 - M_W^2} \left[\bar{u}_s \gamma_\mu (1 - \gamma_5) u_c\right] \left[\bar{v}_u \gamma^\mu (1 - \gamma_5) v_d\right], \tag{2.19}$$

where $u_i$ and $v_i$ are quark spinors and $\gamma_\mu$ and $\gamma_5$ are Dirac matrices. We can then rewrite the amplitude to

$$A = \frac{G_F}{\sqrt{2}} V_{cs}^* V_{ud} \left[\bar{u}_s \gamma_\mu (1 - \gamma_5) u_c\right] \left[\bar{v}_u \gamma^\mu (1 - \gamma_5) v_d\right] + \mathcal{O}(\frac{k^2}{M_W^2}). \tag{2.20}$$

If we look back at Tables 2.1 and 2.3, we can see that the mass of the W boson is well over an order of magnitude higher than most hadrons. As such the momentum transfer

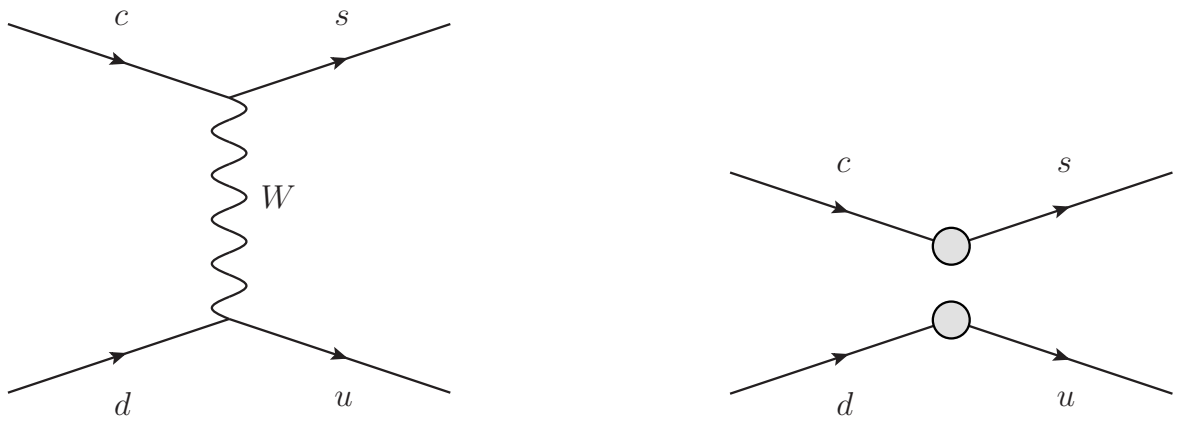


(a) (b)

Figure 2.6: $c \to su\bar{d}$ transition. (a) shows the full diagram, (b) shows the same diagram with the W boson integrated out.

$k$ will be much smaller than the W-boson mass. Therefore we can neglect the $\mathcal{O}(k^2/M_W^2)$ term and still get a good approximation for the transition amplitude $A$. Effectively this comes down to integrating out or "contracting" the W-boson in the Feynman diagram and approximating the interaction as a 4 point interaction, as shown in Fig 2.6.

Considering that these interactions have a low momentum transfer we also need to take into account short distance QCD corrections from gluons entering these diagrams. Fig. 2.7 shows possible gluon couplings for the $c \to su\bar{d}$ example that we used before. From the transition amplitude in (2.20) we can write down the effective Hamiltonian corresponding to the contracted diagram, once again not taking into account QCD corrections,

$$\mathcal{H}_{eff} = \frac{G_f}{\sqrt{2}} V_{cs}^* V_{ud} (\bar{s}c)_{V-A} (\bar{u}d)_{V-A}, \tag{2.21}$$

with the operator

$$(\bar{q}p)_{V-A} \equiv \bar{q}\gamma_\mu(1-\gamma_5)p, \tag{2.22}$$

denoting a vector - axial vector current. If we want to be more precise we can include color indices $\alpha$ and $\beta$ for the quarks and get

$$\mathcal{H}_{eff} = \frac{G_f}{\sqrt{2}} V_{cs}^* V_{ud} (\bar{s}_\alpha c_\alpha)_{V-A} (\bar{u}_\beta d_\beta)_{V-A}. \tag{2.23}$$

If we consider short distance QCD corrections the colour structures of the quark currents can be altered. In order to apply these corrections we can generalize the Hamiltonian to

$$\mathcal{H}_{eff} = \frac{G_F}{\sqrt{2}} V_{cs}^* V_{ud} (C_1(\mu) Q_1 + C_2(\mu) Q_2), \tag{2.24}$$

where

$$Q_1 = (\bar{s}_\alpha c_\beta)_{V-A} (\bar{u}_\beta d_\alpha)_{V_A}, \tag{2.25}$$

$$Q_2 = (\bar{s}_\alpha c_\alpha)_{V-A} (\bar{u}_\beta d_\beta)_{V-A}. \tag{2.26}$$

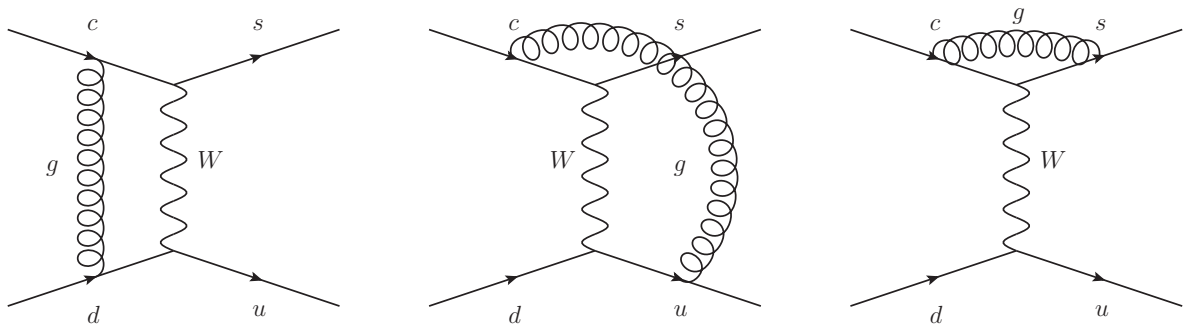


(a) (b) (c)

Figure 2.7: One-loop diagrams showing possible gluon couplings in the $c \to su\bar{d}$ transition. The resulting colour structure in (a) and (b) can be described with operator $Q_1$ and the colour structure in (c) can be described with operator $Q_2$.

We have now expanded the operators to include QCD corrections. The coefficients $C_1$ and $C_2$ serve as the effective coupling constants for the contracted 4 point interactions and are dependent on the strong coupling constant $\alpha_s$, $M_W$ and the renormalization scale $\mu$. These coefficients are called Wilson coefficients. The process of OPE can be applied to any diagram that features heavy particles running internally in the diagrams. Notably this includes higher order diagrams such as the box or penguin diagram. Repeating the process of QCD corrections for these diagrams yields their own set of operators with associated Wilson coefficients. In the case of penguin diagrams, applying OPE to them yields 8 different penguin operators, $Q_3$ through $Q_{10}$, featuring combinations of $V - A$ and $V + A$ currents.

The effective Hamiltonian can be used to calculate the transition amplitude of a given decay channel. This is done by sandwiching $\mathcal{H}_{eff}$ between the initial and final state operators. As an example, let us consider the decay of a neutral B meson $B_q^0$ into a final state $f$. The transition amplitude can then be expressed as

$$A(B_q^0 \to f) = \langle f|\mathcal{H}_{eff}|B_q^0\rangle. \tag{2.27}$$

Later on in this chapter we will see an example of this when we apply the formalism in full.

## 2.3 CP asymmetries and penguin contributions

Now we have all the tools needed to continue with the formalism with which we describe the penguin contributions in neutral $B$ decays. What follows below will be in line with the formalism as introduced in the 2015 paper [18]. This paper discusses both pseudos-scalar-vector final states as well as vector-vector final states. Both cases are largely similar, but the vector-vector case requires one to take polarisation of the transition amplitudes into account.

Starting off, the strength of CP violation in any given decay is given by the CP-violating asymmetry of the decay:

$$a_{CP} \equiv \frac{|A_f(t)|^2 - |\bar{A}_f(t)|^2}{|A_f(t)|^2 + |\bar{A}_f(t)|^2} = \frac{\mathcal{A}_{\mathrm{CP}}^{\mathrm{dir}} \cos(\Delta M_q t) + \mathcal{A}_{\mathrm{CP}}^{\mathrm{mix}} \sin(\Delta M_q t)}{\cosh(\Delta\Gamma_q t/2) - \mathcal{A}_{\Delta\Gamma} \sinh(\Delta\Gamma_q t/2)}, \tag{2.28}$$

where

$$|\overset{(-)}{A}_f(t)|^2 = \Gamma(\overset{(-)}{B}{}^0_q(t) \to f) \tag{2.29}$$

is the time dependent decay rate of a given decay channel. The time dependence is required in order to account for $B^0 - \bar{B}^0$ mixing. In order to show how $a_{\mathrm{CP}}$ leads to the analysis of $\phi_q$ by using the penguin diagrams let's start by deriving the RH side of (2.28). There are several ways to go about this, depending on the definition of $\Gamma(t)$. Here the definition as given in [31] is used:

$$\Gamma(\overset{(-)}{B}{}^0_q(t) \to f) = \left[|g^{(q)}_{\mp}(t)|^2 + |\xi^{(q)}_f|^2 |g^{(q)}_{\pm}(t)|^2 - 2\mathrm{Re}\{\xi^{(q)}_f g^{(q)}_{\pm}(t) g^{(q)}_{\mp}(t)^*\}\right] \tilde{\Gamma}_f, \tag{2.30}$$

where $\tilde{\Gamma}_f$ is the time independent decay rate, which will end up cancelling in the expression for $a_{\mathrm{CP}}$,

$$\left|g^{(q)}_{\pm}(t)\right|^2 = \frac{1}{4}\left[e^{-\Gamma^{(q)}_L t} + e^{-\Gamma^{(q)}_H t} \pm 2e^{-\Gamma^{(q)} t}\cos\left(\Delta M_q t\right)\right], \tag{2.31}$$

$$g^{(q)}_{-}(t) g^{(q)}_{+}(t)^* = \frac{1}{4}\left[e^{-\Gamma^{(q)}_L t} - e^{-\Gamma^{(q)}_H t} \pm 2ie^{-\Gamma^{(q)} t}\sin\left(\Delta M_q t\right)\right], \tag{2.32}$$

and

$$\xi^{(q)}_f = e^{-i\Theta^{(q)}_{M_{12}}} \frac{A(\overline{B^0_q} \to f)}{A(B^0_q \to f)}. \tag{2.33}$$

The angle $\Theta$ in $\xi^{(q)}_f$ is given by

$$\Theta^{(q)}_{M_{12}} = \pi + 2\arg(V^*_{tq} V_{tb}) - \phi_{\mathrm{CP}}(B_q). \tag{2.34}$$

By expressing the time independent transition amplitudes $A(B^0_q \to f)$ in terms of the effective Hamiltonian it is possible to rewrite (2.33) and get

$$\xi^{(q)}_f = -\eta_f e^{-i\phi_q} \frac{A(\overline{B^0_q} \to f)}{A(B^0_q \to f)}. \tag{2.35}$$

Inserting (2.30) into (2.28) and rewriting (a lot) gives

$$a_{\mathrm{CP}} = \frac{\frac{1-|\xi^{(q)}_f|^2}{1+|\xi^{(q)}_f|^2} e^{-\Gamma_q t}\cos(\Delta M_q t) + \frac{2\mathrm{Im}(\xi^{(q)}_f)}{1+|\xi^{(q)}_f|^2} e^{-\Gamma_q t}\sin(\Delta M_q t)}{\frac{1}{2}\left[e^{-\Gamma^{(q)}_L t} + e^{-\Gamma^{(q)}_H t} - \frac{2\mathrm{Re}(\xi^{(q)}_f)}{1+|\xi^{(q)}_f|^2}(e^{-\Gamma^{(q)}_L t} - e^{-\Gamma^{(q)}_H t})\right]}. \tag{2.36}$$

Since $\Gamma_q = \frac{\Gamma^{(q)}_L + \Gamma^{(q)}_H}{2}$ it is possible to rewrite this further and get

$$a_{\mathrm{CP}} = \frac{\frac{1-|\xi^{(q)}_f|^2}{1+|\xi^{(q)}_f|^2}\cos(\Delta M_q t) - \frac{2\mathrm{Im}(\xi^{(q)}_f)}{1+|\xi^{(q)}_f|^2}\sin(\Delta M_q t)}{\cosh(\Delta\Gamma_q t/2) - \frac{2\mathrm{Re}(\xi^{(q)}_f)}{1+|\xi^{(q)}_f|^2}\sinh(\Delta\Gamma_q t/2)} \tag{2.37}$$

Now defining

$$\mathcal{A}^{\mathrm{dir}}_{\mathrm{CP}} \equiv \frac{1-|\xi^{(q)}_f|^2}{1+|\xi^{(q)}_f|^2}, \quad \mathcal{A}^{\mathrm{mix}}_{\mathrm{CP}} \equiv \frac{2\mathrm{Im}(\xi^{(q)}_f)}{1+|\xi^{(q)}_f|^2} \text{ and } \mathcal{A}_{\Delta\Gamma} \equiv \frac{2\mathrm{Re}(\xi^{(q)}_f)}{1+|\xi^{(q)}_f|^2} \tag{2.38}$$

once again gives (2.28). In order to estimate the contribution of the penguin diagrams we can rewrite the time-independent transition amplitudes as follows [14]:

$$A(B_q^0 \to f) \equiv A_f = \quad \mathcal{N}_f[1 - b_f e^{i\rho_f} e^{+i\gamma}], \tag{2.39}$$

and

$$A(\bar{B}_q^0 \to f) \equiv \bar{A}_f = \eta_f \mathcal{N}_f[1 - b_f e^{i\rho_f} e^{-i\gamma}]. \tag{2.40}$$

Here $\eta_f$ is the CP-eigenvalue of the final state $f$, $\mathcal{N}_f$ is a CP conserving factor transcribing the tree diagrams, $b_f$ is a parameter for the strength of the penguin diagrams, $\rho_f$ is a parameter for the CP-conserving strong phase difference between the tree and penguin diagrams and their relative weak phase is given by the UT angle $\gamma$. Apart from $\gamma$ all of these parameters are dependent on the initial and final state particles involved in the decay. They can be written out for a specific decay channel by using OPE, in the process introducing CKM factors and hadronic matrix elements, which will be shown later on.

By inserting (2.39) and (2.40) into (2.35) and using the definitions in (2.38) we can rewrite the direct and mixing induced CP asymmetries in terms of the penguin parameters $b_f$ and $\rho_f$ and the CKM angle $\gamma$:

$$\mathcal{A}_{\mathrm{CP}}^{\mathrm{dir}}(B_q \to f) = \frac{2b_f \sin\rho_f \sin\gamma}{1 - 2b_f \cos\rho_f \cos\gamma + b_f^2}, \tag{2.41}$$

$$\mathcal{A}_{\mathrm{CP}}^{\mathrm{mix}}(B_q \to f) = \eta_f \left[\frac{\sin\phi_q - 2b_f \cos\rho_f \sin(\phi_q + \gamma) + b_f^2 \sin(\phi_q + 2\gamma)}{1 - 2b_f \cos\rho_f \cos\gamma + b_f^2}\right], \tag{2.42}$$

and

$$\mathcal{A}_{\Delta\Gamma}(B_q \to f) = -\eta_f \left[\frac{\cos\phi_q - 2b_f \cos\rho_f \cos(\phi_q + \gamma) + b_f^2 \cos(\phi_q + 2\gamma)}{1 - 2b_f \cos\rho_f \cos\gamma + b_f^2}\right]. \tag{2.43}$$

In order to get a handle on the effect that the penguin topologies have on $\phi_q$ we can use the following equation:

$$\frac{\eta_f \mathcal{A}_{\mathrm{CP}}^{\mathrm{mix}}(B_q \to f)}{\sqrt{1 - (\mathcal{A}_{\mathrm{CP}}^{\mathrm{dir}}(B_q \to f))^2}} = \sin(\phi_q + \Delta\phi_q^f) \equiv \sin(\phi_{q,f}^{\mathrm{eff}}), \tag{2.44}$$

By reordering this expression and introducing (2.42) the following expressions can be derived:

$$\sin\Delta\phi_q^f = \frac{-2b_f \cos\rho_f \sin\gamma + b_f^2 \sin 2\gamma}{(1 - 2b_f \cos\rho_f \cos\gamma + b_f^2)\sqrt{1 - (\mathcal{A}_{\mathrm{CP}}^{\mathrm{dir}}(B_q \to f))^2}}, \tag{2.45}$$

$$\cos\Delta\phi_q^f = \frac{1 - 2b_f \cos\rho_f \cos\gamma + b_f^2 \cos 2\gamma}{(1 - 2b_f \cos\rho_f \cos\gamma + b_f^2)\sqrt{1 - (\mathcal{A}_{\mathrm{CP}}^{\mathrm{dir}}(B_q \to f))^2}}, \tag{2.46}$$

which can be combined to yield

$$\tan\Delta\phi_q^f = -\left[\frac{2b_f \cos\rho_f \sin\gamma - b_f^2 \sin 2\gamma}{1 - 2b_f \cos\rho_f \cos\gamma + b_f^2 \cos 2\gamma}\right] \tag{2.47}$$

Now it is possible to calculate the size of the phase shift $\Delta\phi_f^q$ for a given decay channel. First $b_f$ and $\rho_f$ can be obtained by fitting them to measured values of $\mathcal{A}_{\mathrm{CP}}^{\mathrm{dir}}$ and $\mathcal{A}_{\mathrm{CP}}^{\mathrm{mix}}$

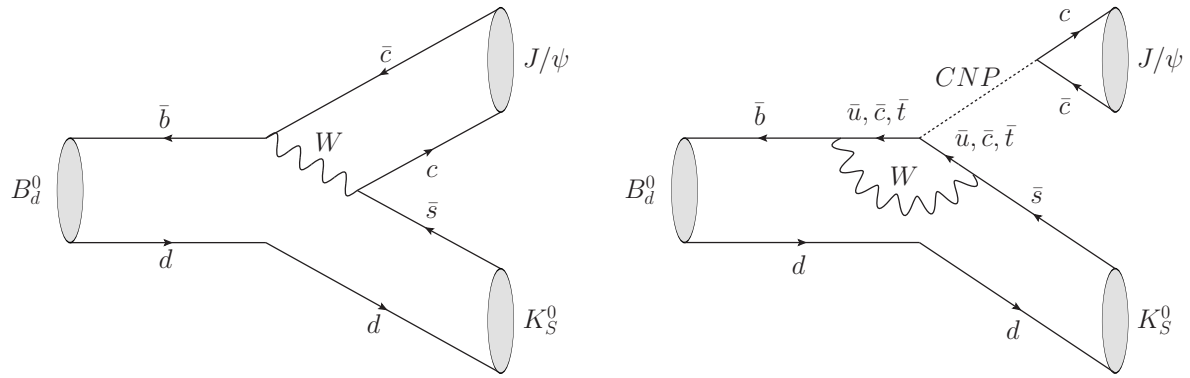


Figure 2.8: Feynman diagrams of the $B_d^0 \to J/\psi K_S^0$ decay channel. (a) shows the tree diagram of the decay featuring a simple W exchange. (b) shows the penguin diagram(s) of the decay, where CNP is once again a colour neutral propagator.

using (2.41) and (2.42). Then using (2.47) $\Delta\phi_q^f$ can be calculated. Note however that this requires $\phi_q$ as an external input in order to make the fit to the penguin parameters. Whilst this is certainly a viable approach it would require multiple iterations since the phase shift that is calculated needs to be applied to $\phi_q$ in order to get the correct results. In the end the values for $b_f$, $\rho_f$ and $\Delta\phi_q^f$ should converge. Later on I will discuss an alternative method that was proposed in the 2015 paper on this topic, which does not require $\phi_q$ as an external input.

## 2.4 Applying the formalism

Now that the general formalism is in place we can apply it to the decay channels that I will be analysing in this thesis. I will start by looking at $B_d^0 \to J/\psi K_S^0$ and deriving the time independent transition amplitude as given in [18], in the end we will arrive at an expression along the lines of (2.39). This decay features a $\bar{b} \to \bar{c}c\bar{s}$ quark level transition that can proceed via a tree topology or via penguin topologies with up-type quark exchanges, the corresponding Feynman diagrams are shown in Fig. 2.8. Using OPE we can express the effective Hamiltonian for these transitions as

$$\mathcal{H}_{eff} = \frac{G_F}{\sqrt{2}} \left[ V_{cb}^* V_{cs} \sum_{k=1}^{2} C_k(\mu) Q_k + \sum_{r=u,c,t} V_{rb}^* V_{rs} \sum_{k=3}^{10} C_k(\mu) Q_k \right]. \tag{2.48}$$

Inserting the Hamiltonian as in (2.27) yields the following transition amplitude for the tree level diagram

$$A_{\text{tree}}(B_d^0 \to J/\psi K_S^0) = \frac{G_F}{\sqrt{2}} V_{cb}^* V_{cs} \langle J/\psi | \sum_{k=1}^{2} C_k(\mu) Q_k | B_d^0 \rangle, \tag{2.49}$$

and for the penguin diagrams

$$A_{\text{penguin}}(B_d^0 \to J/\psi K_S^0) = \sum_{r=u,c,t} \frac{G_f}{\sqrt{2}} V_{rb}^* V_{rs} \langle J/\psi | \sum_{k=3}^{10} C_k(\mu) Q_k | B_d^0 \rangle. \tag{2.50}$$

We can simplify these equations further by defining

$$C' = \frac{G_F}{\sqrt{2}}\langle J/\psi|\sum_{k=1}^{2} C_k(\mu)Q_k|B_d^0\rangle, \text{ and } P'^{(r)} = \frac{G_F}{\sqrt{2}}\langle J/\psi|\sum_{k=3}^{10} C_k(\mu)Q_k|B_d^0\rangle \tag{2.51}$$

where $r \in u, c, t$ denotes the up type quarks running in the penguin diagrams. The primes are there as a reminder that this is a $\bar{b} \to \bar{c}c\bar{s}$ quark level transition. From here we can construct the overall transition amplitude which is now given by

$$A(B_d^0 \to J/\psi K_S^0) = V_{cb}^* V_{cs} C' + \sum_{r\in u,c,t} V_{rb}^* V_{rs} P'^{(r)}. \tag{2.52}$$

Now define $\lambda_r \equiv V_{rb}^* V_{rs}$ to get

$$A(B_d^0 \to J/\psi K_S^0) = \lambda_c C' + \lambda_u P'^{(u)} + \lambda_c P'^{(c)} + \lambda_t P'^{(t)}. \tag{2.53}$$

Next recall the UT relation (2.18) to write $\lambda_t = -\lambda_u - \lambda_c$ and get

$$A(B_d^0 \to J/\psi K_S^0) = \lambda_c \left(C' + P'^{(c)} - P'^{(t)}\right) + \lambda_u \left(P'^{(u)} - P'^{(t)}\right), \tag{2.54}$$

finally divide out $\lambda_c \left(C' + P'^{(c)} - P'^{(t)}\right)$:

$$A(B_d^0 \to J/\psi K_S^0) = \lambda_c \left(C' + P'^{(c)} - P'^{(t)}\right)\left(1 + \frac{\lambda_u}{\lambda_c}\left[\frac{P'^{(u)} - P'^{(t)}}{C' + P'^{(c)} - P'^{(t)}}\right]\right). \tag{2.55}$$

Using (2.15) we can write

$$V_{ub}^* = R_b e^{i\gamma}\frac{|V_{cd}V_{cb}^*|}{V_{ud}}, \tag{2.56}$$

if we now recall that

$$\frac{\lambda_u}{\lambda_c} = \frac{V_{us}V_{ub}^*}{V_{cs}V_{cb}^*}, \tag{2.57}$$

we can insert (2.56) to get

$$\frac{\lambda_u}{\lambda_c} = \frac{V_{us}}{V_{cs}V_{cb}^*}\frac{|V_{cd}V_{cb}^*|}{V_{ud}} R_b e^{i\gamma}. \tag{2.58}$$

Now we can enter the values for the CKM elements by using the Wolfenstein parameterisation, neglecting terms of $\mathcal{O}(\lambda^4)$ or higher yields

$$\frac{\lambda_u}{\lambda_c} = \frac{\lambda^2}{1-\lambda^2} R_b e^{i\gamma}. \tag{2.59}$$

Combining this with the transition amplitude we can write

$$A = \left(1 - \frac{\lambda^2}{2}\right) A\lambda^2 \left(C' + P'^{(u)} - P'^{(t)}\right)\left(1 + \frac{\lambda^2}{1-\lambda^2} R_b e^{i\gamma}\left[\frac{P'^{(u)} - P'^{(t)}}{C' + P'^{(c)} - P'^{(t)}}\right]\right). \tag{2.60}$$

If we now define

$$\mathcal{A}' \equiv A\lambda^2 \left(C' + P'^{(u)} - P'^{(t)}\right), \quad \epsilon \equiv \frac{\lambda^2}{1-\lambda^2}, \tag{2.61}$$

and

$$a'e^{i\theta'} \equiv R_b \left[ \frac{P'^{(u)} - P'^{(t)}}{C' + P'^{(c)} - P'^{(t)}} \right], \tag{2.62}$$

we can finally express the transition amplitude for $B_d^0 \to J/\psi K_S^0$ as

$$A(B_d^0 \to J/\psi K_S^0) = \left(1 - \frac{\lambda^2}{2}\right) \mathcal{A}' \left[1 + \epsilon a' e^{i\theta'} e^{i\gamma}\right]. \tag{2.63}$$

Looking back at (2.39) we can see that $b_f e^{i\rho_f} = -\epsilon a' e^{i\theta'}$ and $\mathcal{N}_f = \left(1 - \frac{\lambda^2}{2}\right)\mathcal{A}'$. A unique feature of all decays featuring the $\bar{b} \to \bar{c}c\bar{s}$ quark level transition, is that the penguin diagrams are doubly Cabibbo suppressed compared to the tree level diagrams. This suppression is parametrized by the parameter $\epsilon$ in the formula above.

The decay channels $B_s^0 \to J/\psi K_S^0$ and $B_d^0 \to J/\psi \pi^0$ both proceed via a $\bar{b} \to \bar{c}c\bar{d}$ transition. The derivation of transition amplitude for these two decays is largely similar as the derivation I did for $B_s^0 \to J/\psi K_S^0$. As such we can arrive at the transition amplitude for the $\bar{b} \to \bar{c}c\bar{d}$ by swapping out the CKM elements. We can do so by making the change

$$V_{rs} \to V_{rd}, \tag{2.64}$$

so now we have

$$\lambda_r^d = V_{rb}^* V_{rd}. \tag{2.65}$$

With this change, the overall factor in front becomes

$$\lambda_r^d \left(C + P^{(c)} - P^{(t)}\right) = -\lambda \cdot A\lambda^2 \left(C + P^{(c)} - P^{(t)}\right), \tag{2.66}$$

The factor $\lambda_u/\lambda_c$ inside the brackets becomes

$$\frac{\lambda_u^d}{\lambda_c^d} = \frac{V_{ud}}{V_{cd}V_{cb}^*} \frac{|V_{cd}V_{cb}^*|}{V_{ud}} R_b e^{i\gamma} = -1 R_b e^{i\gamma}. \tag{2.67}$$

So now the overall transition amplitude for $\bar{b} \to \bar{c}c\bar{d}$ channels becomes

$$A(\bar{b} \to \bar{c}c\bar{d}) = -\lambda\mathcal{A}\left[1 - ae^{i\theta}e^{i\gamma}\right], \tag{2.68}$$

The definitions of the parameters $\mathcal{A}$ and $ae^{i\theta}$ are the same as their primed counterparts, apart from the primes labeling the hadronic matrix elements $C$ and $P^{(q)}$. Furthermore, the Cabbibo suppression of the penguin diagrams compared to the tree diagram is no longer present in these decays, but the overall amplitude is suppressed by a factor $\lambda$. So whilst the overall BR of these decays will be lower, they will be more sensitive to the penguin contributions.

Now that we have the expressions in place for both decay classes ($b \to d$ or $b \to s$ transitions), we can enter this information into the expression for $\tan\Delta\phi_q^f$. For $b \to d$ transitions we have made the replacement $b_f e^{i\rho_f} \to ae^{i\theta}$ to get

$$\tan\Delta\phi_q^f = \frac{-2a\cos\theta\sin\gamma + a^2\sin 2\gamma}{1 - 2a\cos\theta\cos\gamma + a^2\cos 2\gamma}, \tag{2.69}$$

using a Taylor expansion in $a$ this can be simplified to

$$\tan\Delta\phi_q^f = -2a\cos\theta\sin\gamma - a^2\cos 2\theta\sin 2\gamma + \mathcal{O}(a^3). \tag{2.70}$$

For $b \to s$ transitions we need to make the replacement $b_f e^{i\rho_f} = -\epsilon a' e^{i\theta'}$, which yields

$$\tan \Delta\phi_q^f = \frac{2\epsilon a' \cos\theta' \sin\gamma + \epsilon^2 a'^2 \sin 2\gamma}{1 + 2\epsilon a' \cos\theta' \cos\gamma + \epsilon^2 a'^2 \cos 2\gamma} = 2\epsilon a' \cos\theta' \sin\gamma + \mathcal{O}(\epsilon^2 a'^2), \tag{2.71}$$

where we can once again use a Taylor expansion to simplify the equation. An important note here is that the decay channel determines which angle can be measured, regardless of the quark transition involved in the decay channel in question. Therefore the formulas given above can apply to both $\phi_s$ and $\phi_d$, rather than exclusively to one or the other. To give an example of this consider the $B_s^0 \to J/\psi K_S^0$ and $B_d^0 \to J/\psi\pi^0$ decay channels. Both channels feature a $\bar{b} \to \bar{c}c\bar{d}$ quark level transition, but $B_s^0 \to J/\psi K_S^0$ probes $\phi_s$ whereas $B_d^0 \to J/\psi\pi^0$ probes $\phi_d$, so for both decay channels Eq. (2.70) should be used. As is pointed out in Ref. [18] the equations both depend on the strong phase difference $\theta^{(\prime)}$ in the same way. So in general, the penguin induced phase shifts will be largest with a strong phase difference of 0° or 180° and will be smallest at 90° and 270°.

## 2.5 Branching Ratio information

Before I move on to explain how we can use the formalism introduced in the sections above to perform measurements on $\phi_s$ and $\phi_d$ there is one more topic I would like to bring up which has to do with U-spin symmetry in strong interactions, which is also referred to as $SU(3)$ symmetry. U-spin symmetry states that strong interactions do not change when interchanging $s$ and $d$ quarks. If we consider that the penguin parameters $a$ and $\theta$ depend on QCD operators introduced by OPE it is easy to see that under U-spin symmetry we have

$$a' e^{i\theta'} = a e^{i\theta}, \tag{2.72}$$

and

$$\mathcal{A}' = \mathcal{A}. \tag{2.73}$$

These relations become very useful if we consider that the penguins in $\bar{b} \to \bar{c}c\bar{s}$ transitions are suppressed compared to tree level by a factor $\epsilon \approx 0.05$. U-spin symmetry would allow for using the magnified penguins featured in $\bar{b} \to \bar{c}c\bar{d}$ transitions to probe the contribution coming from suppressed penguins. This would allow for a iterative approach towards determining $\phi_s$ and $\phi_d$.

Looking at the equations for $A_{\text{dir}}$ and $A_{\text{mix}}$ we can see that in order to obtain a good measurement of the penguin parameters, the weak phase difference $\phi_q$ is needed, simultaneously the penguin parameters are required to obtain the weak phase shifts $\Delta\phi_q$. By using U-spin symmetry we can obtain the penguin parameters in a $B_d$ decay using $\phi_d$ as input and then use the penguin parameters to calculate $\Delta\phi_s$ and subsequently $\phi_s$ in a U-spin symmetric $B_s$ decay and vice versa. This approach however, is not entirely theoretically clean since U-spin is a broken symmetry. So in order to interchange the penguin parameters between the magnified and suppressed penguin diagrams we would first need to make corrections due to U-spin breaking. The size of these corrections can be determined by calculating them in factorisation. Should the U-spin breaking effects prove to be small enough, it is still possible to use (2.72) without any repercussions.

When using factorisation to calculate the penguin parameters the factorisable effects cancel in the ratio of tree and penguin amplitudes, so any U-spin breaking effect will

enter through non-factorisable parts only. However, since $\mathcal{A}$ is not built out of a ratio of amplitudes U-spin breaking effects can enter through factorisation as well. Whilst it is possible to make these calculations in factorisation the accuracy for reproducing the BR of $B \to J/\psi K$ is not great.

So far I have shown a method for obtaining the size of the penguin contributions by looking at the CP-violating amplitudes $A_{\rm mix}$ and $A_{\rm dir}$. It is possible to introduce further constraints on the values for $a$ and $\theta$ by utilizing branching ratio information. Taking $B_s^0 \to J/\psi K_S^0$ as an example, the experimental BR is defined as

$$\mathcal{B}(B_s^0 \to J/\psi K_S^0)_{\rm exp} \equiv \frac{1}{2}\int_0^\infty \langle \Gamma(B_s^0(t) \to J/\psi K_S^0)\rangle dt \tag{2.74}$$

where

$$\langle \Gamma(B_s^0(t) \to J/\psi K_S^0)\rangle = \Gamma(B_s^0(t) \to J/\psi K_S^0) + \Gamma(\bar{B}_s^0(t) \to J/\psi K_S^0). \tag{2.75}$$

The definition of $\Gamma(\overset{(-)}{B}{}_q^0(t) \to f)$ is given in (2.30). Since this BR definition is time-integrated it is important to distinguish it from the theoretical BR which is defined at time $t = 0$. This is especially important if the decay width difference $\Delta\Gamma$ is quite large, which is the case for the $B_s$ system, but not for the $B_d$ system. The size of the decay width difference in $B_s$ can be described by the parameter [32]

$$y_s = \frac{\Delta\Gamma_s}{2\Gamma_s} = 0.0675 \pm 0.004^1 \tag{2.76}$$

The two BR concepts can then be transformed by using

$$\mathcal{B}(B_s^0 \to J/\psi K_S^0)_{\rm theo} = \left[\frac{1-y_s^2}{1+\mathcal{A}_{\Delta\Gamma}(B_s^0 \to J/\psi K_S^0) y_s}\right] \mathcal{B}(B_s^0 \to J/\psi K_S^0)_{\rm exp}. \tag{2.77}$$

We have seen before that $\mathcal{A}_{\Delta\Gamma}$ also depends on the penguin parameters, but it can also be calculated by using the effective lifetime

$$\tau^{\rm eff}_{J/\psi K_S^0} \equiv \frac{\int_0^\infty t\langle \Gamma(B_s(t) \to J/\psi K_S^0)\rangle dt}{\int_0^\infty \langle \Gamma(B_s(t) \to J/\psi K_S^0)\rangle dt} \tag{2.78}$$

$$= \frac{\tau_{B_s}}{1-y_s^2}\left[\frac{1+2\mathcal{A}_{\Delta\Gamma}(B_s^0 \to J/\psi K_S^0) y_s + y_s^2}{1+\mathcal{A}_{\Delta\Gamma}(B_s^0 \to J/\psi K_S^0) y_s}\right]. \tag{2.79}$$

Now we can finally construct the observable in order to use the BR information. The observable is defined as

$$H \equiv \frac{1}{\epsilon}\left|\frac{\mathcal{A}'}{\mathcal{A}}\right|^2 \frac{{\rm PhSp}(B_d^0 \to J/\psi K_S^0)}{{\rm PhSp}(B_s^0 \to J/\psi K_S^0)} \frac{\tau_{B_d}}{\tau_{B_s}} \frac{\mathcal{B}(B_s^0 \to J/\psi K_S^0)_{\rm theo}}{\mathcal{B}(B_d^0 \to J/\psi K_S^0)_{\rm theo}}. \tag{2.80}$$

This can be rewritten in terms of penguin parameters to get

$$H = \frac{1-2a\cos\theta\cos\gamma + a^2}{1+2\epsilon a'\cos\theta'\cos\gamma + \epsilon^2 a'^2} = -\frac{1}{\epsilon}\frac{\mathcal{A}_{\rm CP}^{\rm dir}(B_d^0 \to J/\psi K_S^0)}{\mathcal{A}_{\rm CP}^{\rm dir}(B_s^0 \to J/\psi K_S^0)}. \tag{2.81}$$

[1] HFLAV reports $\Delta\Gamma_s/\Gamma_s = 0.135 \pm 0.008$.

Whilst this observable allows us to put extra constraints on the penguin parameters. It is not a particularly nice observable to use since the ratio $|\mathcal{A}'/\mathcal{A}|$ is affected by the U-spin corrections mentioned above. In turn, this presents us with the opportunity to use the observable $H$ to estimate the size of these U-spin corrections if the penguin parameters are already known. To do this we first need to calculate the ratio $|\mathcal{A}'/\mathcal{A}|$ in factorisation and then compare this value to the ratio obtained from $H$ using both the penguin parameter and the BR information as input. From this estimation it would then be possible to correct (2.72) and use the penguin parameters across decay classes.

# Chapter 3

# Methods

In the previous chapter I discussed the formalism behind controlling the penguin uncertainties in measurements for $\phi_s$ and $\phi_d$. In this chapter I will discuss how we can apply this formalism to obtain the penguin shifts $\Delta\phi_q$ in a clean way. I already mentioned some of the difficulties in finding these phase shifts, but I will be highlighting them here again. After the method for getting these phase shifts is established I will discuss how these methods were applied in practice and what tools were used to get the final results.

## 3.1 Obtaining the penguin parameters

Let's begin with once again listing the difficulties with obtaining the penguin parameters in a clean way before listing the possible solutions to this problem. First and foremost is that in order to obtain the penguin parameters from a single decay channel, the weak mixing phase $\phi_q$ is required as an external input. This is a problem because the addition of the penguin diagrams to the overall analysis introduces a phase shift $\Delta\phi_q$ which modifies the weak mixing phases. From a single decay channel the penguin parameters can be fitted for by using $\mathcal{A}_{\mathrm{CP}}^{\mathrm{dir}}$ and $\mathcal{A}_{\mathrm{CP}}^{\mathrm{mix}}$. The end result is a system with two equations and three variables, because of this, there is no unique solution to this system. In order to properly obtain results it is necessary to introduce additional constraints to the system. Besides getting additional theoretical relations with which to constrain the system there are two approaches that can be taken.

### 3.1.1 Iterative approach

The first approach to getting a proper fit for the penguin parameters is an iterative one. With this approach $\phi_q$ is first entered as an external input, allowing for a fit to the penguin parameters. Using these penguin parameters, $\Delta\phi_q$ can be calculated and corrected for. This process can then be repeated until the fit converges to a single set of values for $\phi_q$, $a$ and $\theta$. Using this approach it is possible to obtain penguin corrections for each individual decay channel, but iterating for $\phi_q$ will take some time. The weak phases that are calculated are associated with $\bar{B}_q^0 - B_q^0$ mixing and should be independent of the specific decay channel that is studied. A sanity check therefore would be to see if the weak phases obtained from iterating over each channel separately converge to the same value. In any case, the weak phases coming from the different decay channels could in the end be averaged to obtain a final result.

The biggest risk in iterating over a single channel is that it uses $\phi_q$ to obtain $\phi_q$, which is highly likely to lead to the wrong results. There are two ways around this problem. If we are trying to obtain the phase $\phi_d$ from $B_d$ decays, the first solution would be to make use of a $B_s$ decay featuring the same quark level transition. Because the transition is the same, the penguin parameters entering both decay channels are the same. This would allow for using the $B_s$ decay with $\phi_s$ as an external input to obtain $a$ and $\theta$, and then use them to calculate $\Delta\phi_d$ and $\phi_d^{\text{eff}}$ using the $B_d$ decay. The second solutions is an extension to the first by making use of $SU(3)$ flavour symmetry of the strong interactions. Using this symmetry one can relate decays featuring Cabbibo suppressed penguins to decay with unsuppressed penguins and vice versa, allowing for a wider array of decays to be used to find the penguin parameters and subsequently $\phi_q$. Iterating over the decay channels back and forth would still be required to see if the values obtained in this way converge.

### 3.1.2 Combined fit approach

Instead of iterating over decay channels in order to obtain values for $\phi_q$ one can also make a simultaneous fit to all parameters. Similar to the case with iteration the best case scenario would be to use decay channels that feature the same the quark level transition, once again from both $B_d$ and $B_s$. This creates a set of four equations, $\mathcal{A}_{\text{CP}}^{\text{dir}}(B_s \to f)$, $\mathcal{A}_{\text{CP}}^{\text{mix}}(B_s \to f)$, $\mathcal{A}_{\text{CP}}^{\text{dir}}(B_d \to f)$ and $\mathcal{A}_{\text{CP}}^{\text{mix}}(B_d \to f)$, and four variables, $a$, $\theta$, $\phi_s$ and $\phi_d$. Because of this a simultaneous fit to all four variables can be made, without needing to iterate to obtain the final results. Also here $SU(3)$ flavour symmetry can be used to expand the scope of decay channels. The challenge with both approaches is to find decay channels of both $B_s$ and $B_d$ with matching quark level transitions with sufficiently high accuracy measurements in order to obtain meaningful results. Whilst for the $B_d$ system there are many measurements of $\mathcal{A}_{\text{CP}}^{\text{dir}}$ and $\mathcal{A}_{\text{CP}}^{\text{mix}}$ for a wide variety of decay channels, this is not the case for the $B_s$ system.

## 3.2 Fitting method

Now that the possible approaches for making the fits for the penguin parameters have been discussed, I will move on to discuss the software that was used to make these fits. Whilst it is doable to write custom code in order to make the fits, it would be nice to write code that is compatible with fitting solutions that are already being employed by other groups. The idea being that it would facilitate those groups in starting to use the formalism presented in this thesis to correct for penguin uncertainties in their analyses. To that end the software package that I used for making the fits for the penguin parameters is GammaCombo. The motivation for this choice is that it is already being used to make fits to CKM parameters from which the mixing phases can be estimated. If GammaCombo is already employed by these groups it can straightforwardly be added to their existing fitting package.

### 3.2.1 GammaCombo

GammaCombo is a software package that was developed by members of the LHCb collaboration for use within the C++ based ROOT library developed at CERN. As the name

implies, GammaCombo is currently being used by the LHCb collaboration for making fits to CKM parameter $\gamma$ [33, 34]. The fits made by GammaCombo are so-called likelihood fits. The fits are constructed by defining probability density functions (PDFs) for the observables and combining these to form a likelihood function. The likelihood $\mathcal{L}$ is given by

$$\mathcal{L}(\vec{\alpha}) = \prod_i \mathcal{L}_i(\vec{\beta}_i), \tag{3.1}$$

where $\alpha$ and $\beta$ are vectors that hold all parameters of the input measurements. The likelihood for any given observable can be obtained from the PDF by fixing the value of the observable to its measured value, so given a PDF of observables $\vec{A}$

$$\text{PDF} = f(\vec{A}|\vec{\beta}) \tag{3.2}$$

the corresponding likelihood is given by

$$\mathcal{L}(\vec{\beta}) = f(\vec{A}|\vec{\beta})\Big|_{\vec{A}=\vec{A}_{obs}}. \tag{3.3}$$

As an example, consider the observable $\mathcal{A}_{\text{CP}}^{\text{dir}}(B_s^0 \to J/\psi K_S^0)$. In this case the parameter vector $\vec{\beta}$ would be given by

$$\vec{\beta} \equiv \begin{pmatrix} a \\ \theta \\ \phi_s \\ \gamma \end{pmatrix}. \tag{3.4}$$

If both $\mathcal{A}_{\text{CP}}^{\text{dir}}$ and $\mathcal{A}_{\text{CP}}^{\text{mix}}$ have been measured, a fit for $a$ and $\theta$ could be made by combining the likelihood of $\mathcal{A}_{\text{CP}}^{\text{dir}}$ with that of $\mathcal{A}_{\text{CP}}^{\text{mix}}$ and giving $\phi_s$ and $\gamma$ as external inputs. The fits made in this way by GammaCombo yield central fit values as well as confidence intervals corresponding to 1 and 2 $\sigma$ deviations from the central value. Using GammaCombo it is possible to combine any number of PDFs into these likelihood fits. This allows for easy addition of new measurements/decay channels in order to improve the fit results. A more detailed description of the fitting method employed by GammaCombo as well as instructions for using this package can be found in the GammaCombo manual available from their website [19].

### 3.2.2 Fitting Module

The fitting module developed in GammaCombo has seen several iterations before the final version with which the results are obtained. The initial approach was to make two separate modules for the different quark level transitions and use the iterative method for obtaining the fit results. This was based mostly on the (incorrect) assumption that each decay class corresponded to its own weak phase. Since this is not the case, setting up the modules in this way introduced quite a lot of duplicate code and made combined fits across decay classes more difficult. The current version uses a single module for all decay classes, eliminating the need for some duplicate code and allowing for easy combined fits of different decay classes as well as being able to quickly add new observables to the global fit.

As mentioned before the module consists of multiple PDFs that are later combined to make the fits. The PDFs are constructed by distinguishing between different "classes"

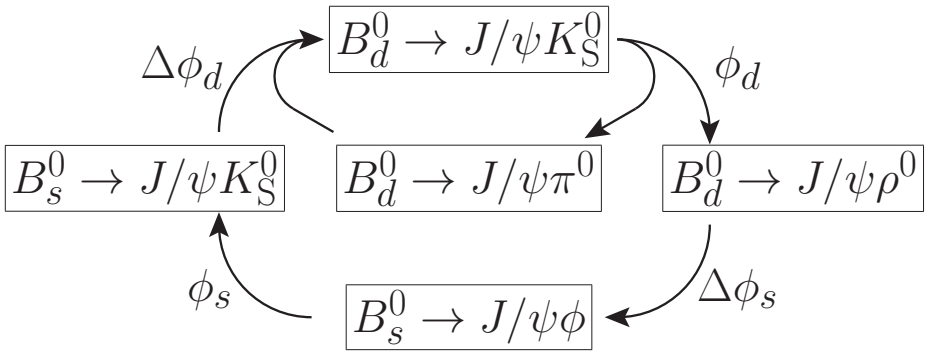


Figure 3.1: Interplay between all decay channels used for obtaining the penguin parameters [35].

of decay channels. The main two classes are those of Pseudo-scalar-Vector (P-V) and Vector-Vector (V-V) final states. In the latter class the polarisation of the final state particles needs to be taken into account. These two classes can then be further divided by separating them into decays featuring suppressed penguins ($\bar{b} \to \bar{c}c\bar{s}$ transitions) and unsuppressed penguins ($\bar{b} \to \bar{c}c\bar{d}$ transitions). For each class we then defined PDFs for $\mathcal{A}_{\rm CP}^{\rm dir}$, $\mathcal{A}_{\rm CP}^{\rm mix}$ as well as the combination of both. This was done so it is possible to see how $\mathcal{A}_{\rm CP}^{\rm dir}$ and $\mathcal{A}_{\rm CP}^{\rm mix}$ each contribute independently to the overall fit. For the PDFs that include $\mathcal{A}_{\rm CP}^{\rm mix}$ we also need to distinguish between $B_d$ and $B_s$ decays because of the dependence of $\mathcal{A}_{\rm CP}^{\rm mix}$ on the mixing phases $phi_s$ and $\phi_d$. By defining the PDFs this way additional decay channels can be quickly added to the analysis if their decay structure is known.

An important point of consideration is the CP-eigenvalue of the final state. Since these values can be different for channels falling within the same decay mode they need to be taken into account. The CP eigenvalues enter $\mathcal{A}_{\rm CP}^{\rm mix}$ as can be seen in (2.42). Instead of having the CP-eigenvalue present in the definition of the theoretical relation used in the fit, it can be multiplied with the observed values for $\mathcal{A}_{\rm CP}^{\rm mix}$. This way it is not necessary to define two separate PDFs for $\mathcal{A}_{\rm CP}^{\rm mix}$ in order to account for odd or even CP-eigenstates. Care needs to be taken however to correctly multiply the observed values reported by experiments, since some experiments might report a value that is already multiplied with $\eta_{\rm CP}$ whilst others do not.

The fitting approach and the decay channels that are used in the GammaCombo module closely match those from the 2015 paper, Ref. [18], on controlling the penguin contributions. In that paper $B_d^0 \to J/\psi K_S^0$, $B_s^0 \to J/\psi K_S^0$, $B_d^0 \to J/\psi\rho^0$ and $B_s^0 \to J/\psi\phi$ were used to make the global fit. This time $B_d^0 \to J/\psi\pi^0$ is also used as an additional control on $B_d^0 \to J/\psi K_S^0$. The interplay between the resulting five decay channels, shown in Fig. 3.1, now works by using the P-V $B_d^0$ channels to find $\phi_d$. This is then used as input for $B_d^0 \to J/\psi\rho^0$ to calculate $\Delta\phi_s$. $\Delta\phi_s$ then corrects the value of $\phi_s$ fitted from $B_s^0 \to J/\psi\phi$. The value for $\phi_s$ then serves as input for $B_s^0 \to J/\psi K_S^0$ in order to find $\Delta\phi_d$ needed to correct $\phi_d$, closing the loop. In the next chapter this interplay between the decay channels is discussed in more detail, also providing the motivation for using $B_d^0 \to J/\psi\pi^0$ as an additional control.

# Chapter 4

# Results

## 4.1 External input parameters

Now that the formalism and the method for obtaining the penguin parameters have been established it is time to make the fits to experimental data and look at the results. In order to make the fits some external input parameters are required. For all fits to penguin parameters the CKM angle $\gamma$ is required. Whilst it is possible to use the penguin fits to obtain a value for $\gamma$ given enough input measurements as was pointed out in previous work [14, 17, 31], doing so now will not yield more accurate results than those obtained by collaborations like CKMfitter and UTFit. The value that will be used here is reported by HFLAV [32] as:

$$\gamma = (71.1^{+4.6}_{-5.3})^\circ. \tag{4.1}$$

In order to make fits to the penguin parameters coming from the doubly Cabbibo suppressed $\bar{b} \to \bar{c}c\bar{s}$ channels the suppression parameter $\epsilon$ is also needed, using Eq. (2.61) and $\lambda \equiv |V_{us}| = 0.2231 \pm 0.0007$ [35] gives

$$\epsilon \equiv \frac{\lambda^2}{1-\lambda^2} = 0.05328 \pm 0.00035. \tag{4.2}$$

Finally the current measurements of the mixing phases $\phi_d$ and $\phi_s$ also need to be given as external input if a fit is being made to a single channel. Afterwards it is then possible to correct this value with the penguin parameters and iterate to get the final result for the mixing phase. As mentioned in the previous chapter it is possible to make simultaneous fits to both the penguin parameters and the mixing phases by utilising multiple decay channels with the same primary particle, in this case either $B^0_d$ or $B^0_s$. Beside the mixing phases being required for the iterative fit approach they also provide a benchmark to compare the results from the penguin parameter formalism against. Starting with the $B^0_d$ mixing phase $\phi_d$, the external input comes from the CKMfitter collaboration based on their measurement of the CKM angle $\beta$. Using that $\phi_d = 2\beta$ and $\beta = (22.14^{+0.69}_{-0.67})^\circ$ [28],

$$\phi_d = (44.28 \pm 1.4)^\circ. \tag{4.3}$$

The $B^0_s$ mixing parameter $\phi_s$ is obtained from the HFLAV collaboration using $B^0_s \to J\psi\phi$, $J/\psi K^+K^-$ and $J/\psi\pi^+\pi^-$ modes. They report (in radians) [32]

$$\phi_s = -0.021 \pm 0.031. \tag{4.4}$$

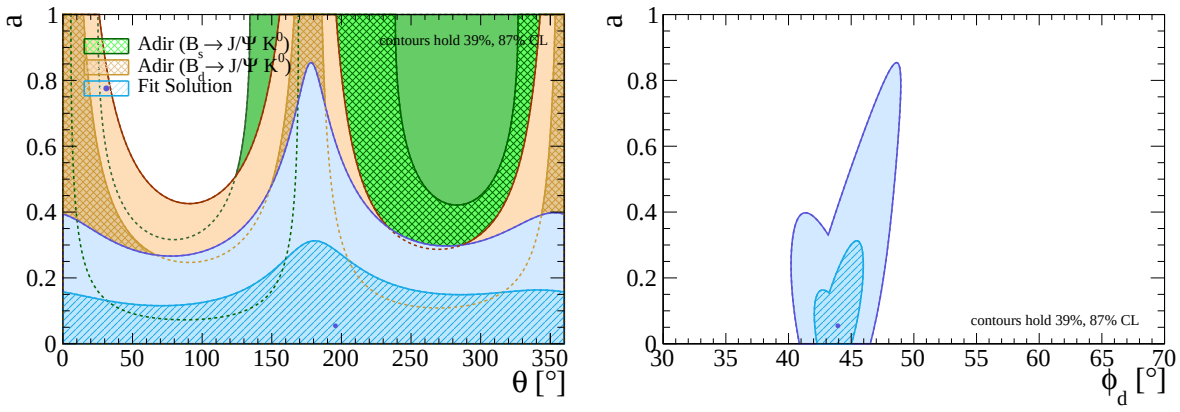


(a) (b)

Figure 4.1: Two-dimensional confidence regions for the combined fit to $B_d^0 \to J/\psi K_S^0$ and $B_s^0 \to J/\psi K_S^0$. (a) shows the confidence region for the fit to $a$ and $\theta$ together with $\mathcal{A}_{\mathrm{CP}}^{\mathrm{dir}}$ from both channels, (b) shows the correlation between $a$ and $\phi_d$ from the combined fit.

## 4.2 Pseudo-scalar - Vector results

For obtaining the mixing phase $\phi_d$, the CP asymmetries from $B_d^0 \to J/\psi K_S^0$ are used. The experimental averages for the CP asymmetries are reported by the HFLAV collaboration as [32][1]:

$$\mathcal{A}_{\mathrm{CP}}^{\mathrm{dir}}(B_d^0 \to J/\psi K_S^0) = -0.007 \pm 0.018, \qquad \eta\mathcal{A}_{\mathrm{CP}}^{\mathrm{mix}}(B_d^0 \to J/\psi K_S^0) = 0.690 \pm 0.018. \quad (4.5)$$

In order to have a clean determination of the penguin parameters additional input is typically obtained from the $SU(3)$ counterpart $B_s^0 \to J/\psi K_S^0$. The latest experimental averages for this channel come from LHCb [36]:

$$\mathcal{A}_{\mathrm{CP}}^{\mathrm{dir}}(B_s^0 \to J/\psi K_S^0) = -0.28 \pm 0.42, \qquad \eta\mathcal{A}_{\mathrm{CP}}^{\mathrm{mix}}(B_s^0 \to J/\psi K_S^0) = 0.08 \pm 0.41. \quad (4.6)$$

Since the errors on these values are still quite large they do not provide a good constraint on the penguin parameters in order to obtain nice results, this can be clearly seen in Fig. 4.1, despite this $B_s^0 \to J/\psi K_S^0$ will be useful later on.

Because $B_s^0 \to J/\psi K_S^0$ does not provide meaningful constraints we have to look elsewhere. In the past [16] $B_d^0 \to J/\psi \pi^0$ has been used as an additional control for extracting penguin parameters from $B_{s,d}^0 \to J/\psi K_S^0$. The same can be done here, which has the added benefit of not needing to use $\phi_s$ and $\phi_d$ as external inputs, instead $\phi_d$ can be obtained directly from the combined fit to both $B_d^0 \to J/\psi K_S^0$ and $B_d^0 \to J/\psi \pi^0$. Once again using the HFLAV average for the CP asymmetries, they report [32]:

$$\mathcal{A}_{\mathrm{CP}}^{\mathrm{dir}}(B_d^0 \to J/\psi \pi^0) = 0.04 \pm 0.12, \qquad \eta\mathcal{A}_{\mathrm{CP}}^{\mathrm{mix}}(B_d^0 \to J/\psi \pi^0) = 0.86 \pm 0.14. \quad (4.7)$$

[1]The results shown here are for $B_d \to J/\psi K^0$ and have been taken from their website. Since the decay to both $K_S$ and $K_L$ feature the same quark transition, their CP asymmetries can be averaged without problem. The only relevant difference between the two decay channels is the CP eigenvalue of the final state which is accounted for in $\eta\mathcal{A}_{\mathrm{CP}}^{\mathrm{mix}}$. See also [35].

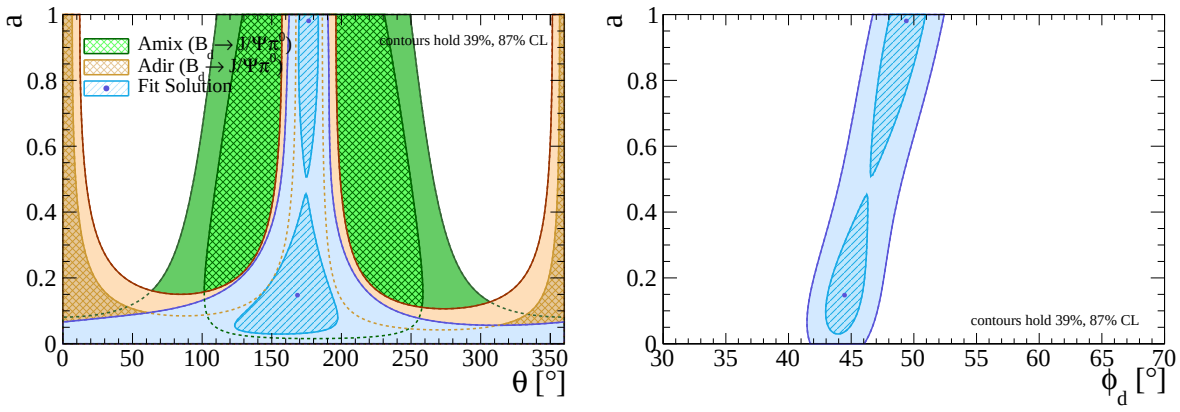


(a) (b)

Figure 4.2: Two-dimensional confidence regions for the combined fit to $B_d^0 \to J/\psi K_S^0$ and $B_d^0 \to J/\psi\pi^0$. (a) shows the CP asymmetries from $B_d^0 \to J/\psi\pi^0$ together with the final fit region for $a$ and $\theta$. (b) shows the correlation between $a$ and $\phi_d$.

When adding either $B_s^0 \to J/\psi K_S^0$ or $B_d^0 \to J/\psi\pi^0$ to the fit, we can assume $SU(3)$ symmetry to get $ae^{i\theta} = \epsilon a' e^{i\theta'}$, allowing for a single solution to the penguin parameters across decay channels. Making the combined fit to $a$, $\theta$ and $\phi_d$ using (4.5) and (4.7) as input yields:

$$a = 0.15^{+0.31}_{-0.12}, \qquad \theta = (168^{+31}_{-47})^\circ, \qquad \phi_d = (44.5^{+1.8}_{-1.5})^\circ. \tag{4.8}$$

The solution for $a$ and $\theta$ then yields

$$\Delta\phi_d = (-0.8^{+0.7}_{-1.8})^\circ. \tag{4.9}$$

The two-dimensional confidence regions for this fit are shown in Fig. 4.2. These fits show that using only the $B_d^0$ channels provides a good result for $\theta$, but there still exists some ambiguity for the value of $a$ as can be seen by a second solution with $a \approx 1$. Fig 4.2b also shows a sizeable correlation between $a$ and $\phi_d$, highlighting the importance of controlling the penguin contributions in order to make more precise measurements. Looking back at (2.62), a value for $a > R_b \approx 0.39$ would imply that the penguin diagrams would have a leading contribution to the overall transition amplitude. This high-valued solution for $a$ would not be a physical one since the penguin diagrams are loop suppressed compared to the tree diagrams, not to mention that the penguin diagrams in $B_d^0 \to J/\psi K_S^0$ are doubly Cabbibo suppressed as well resulting in an even smaller transition amplitude. Therefore, the transition amplitude of the tree diagram will always be larger than the penguin diagram amplitude. Based on this, a large value for $a$ as shown by the second solution in Fig. 4.2 is heavily disfavoured compared to the solution with $a < R_b$.

Whilst we can solve the ambiguity shown here based on physical reasons it would be better to try and remove it entirely. This can be done by adding more constraints in the form of either theoretical relations or by including more decay channel information. Whilst the $B_s^0 \to J/\psi K_S^0$ channel by itself can not provide meaningful results due to the large uncertainty coming from the experiments, it could be used to try and eliminate the large valued solution for $a$ shown in the fit. Including $B_s^0 \to J/\psi K_S^0$ can be done based on $SU(3)$ relations but it does require the use of $\phi_s$ as external input. Even so, it does provide an unambiguous result for $a$ and $\theta$ as will be seen later on in 4.4.

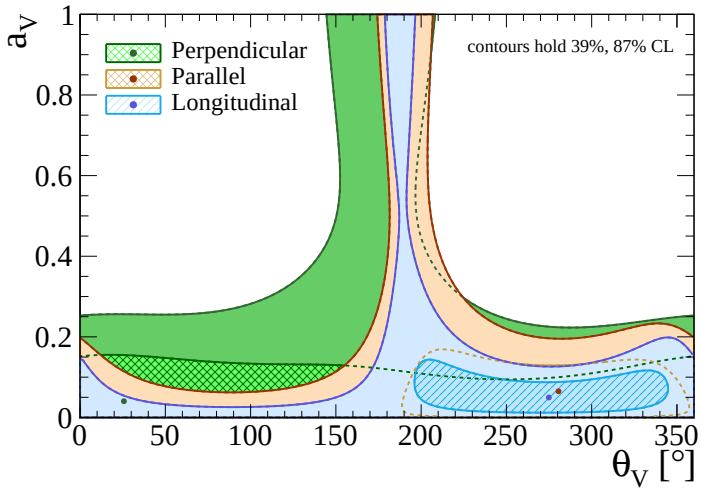


Figure 4.3: Two-dimensional confidence regions of the angular penguin parameter fit solutions for each of the polarisation states.

## 4.3 Vector - Vector results

Whilst the introduction of $B_s^0 \to J/\psi K_S^0$ to the $B_d^0 \to J/\psi X$ fit removes the ambiguity present in that fit, it does introduce $\phi_s$ as an external input. Since this once again would introduce iteration to the fitting process it would be useful to try and avoid this and find a method for fitting for $\phi_s$ together with the other parameters. Once again looking at the past [15, 18], the decay channel $B_s \to J/\psi\phi$ has been used to measure the penguin contributions to $\phi_s$ and the same can be done here as well. The penguin parameters coming from the V-V decay channels are labeled $a_V$ and $\theta_V$. As with the P-V fits, it is useful to introduce a control channel in order to make a simultaneous fit to both the penguin parameters and the mixing phase. The P-V modes can not be used for this because of the different decay dynamics. As mentioned briefly in both the Theory and the Methods chapters, the V-V final states feature two vector mesons in their final states which requires the use of polarisation states in order to describe the decay dynamics. It is possible to make a polarisation independent fit if the required CP asymmetries are known, but the penguin parameters resulting from this fit can still not be compared to the ones featured in the P-V fits above. The mixing phase(s) obtained from the V-V fit are still the same $B_q^0 \leftrightarrow \bar{B}_q^0$ mixing phases that are found using the P-V fits. Because of this polarisation of the penguin parameters, the control channel should also feature a V-V final state. Once again, we can look at the $SU(3)$ partner of this decay channel for our control which in this case is $B_d^0 \to J/\psi\rho$. Including these two decay channels to the overall fit now allows for a global fit to all parameters of interest, an the external input parameters are now reduced to $\epsilon$ and $\gamma$. The polarisation dependent CP-asymmetries of $B_s^0 \to J/\psi\phi$ are not available from experiments so they were obtained by calculating their values based on current measurements of $\phi_{s,J/\psi\phi}^{eff}$ [35]. They come out to be

$$\mathcal{A}_{\rm CP}^{\rm dir}(B_s^0 \to J/\psi\phi) = 0.006 \pm 0.013, \qquad \eta\mathcal{A}_{\rm CP}^{\rm mix}(B_s^0 \to J/\psi\phi) = -0.085 \pm 0.025. \quad (4.10)$$

For $B_d^0 \to J/\psi\rho^0$ the polarisation dependent CP asymmetries have been measured, allowing for a comparison of the V-V penguin parameters obtained from the polarisation

states. The results of this comparison are shown in Fig. 4.3 which shows that with current precision for the polarisation dependent CP asymmetries all results are in agreement with one another and no polarisation dependent effects can be measured. For now we can continue with the global fit by using the polarisation independent CP asymmetries for $B_d^0 \to J/\psi\rho^0$ which are given by [37]

$$\mathcal{A}_{\rm CP}^{\rm dir}(B_d^0 \to J/\psi\rho^0) = -0.064 \pm 0.059, \qquad \eta\mathcal{A}_{\rm CP}^{\rm mix}(B_d^0 \to J/\psi\rho^0) = 0.66 \pm 0.15. \quad (4.11)$$

## 4.4 Global fit results

If we now were to make a fit to the V-V channels by themselves we would once again require external input for the mixing phase $\phi_d$. Unlike the situation with $\phi_s$ in the P-V fits above, we can now make use of the P-V fits to obtain $\phi_d$ as an input for the V-V fit. As already mentioned in Chapter 3 and shown in Fig. 3.1, the global fit now works by using $B_d^0 \to J/\psi K_S^0$ and $B_d^0 \to J/\psi\pi^0$ to obtain $\phi_d$, which is than used as input for $B_d^0 \to J/\psi\rho^0$. From here $\Delta\phi_s$ can be estimated and used to obtain $\phi_s$ from $B_s^0 \to J/\psi\phi$. $\phi_s$ is then used as input to obtain penguin parameters from $B_s^0 \to J/\psi K_S^0$ in order to find $\Delta\phi_d$ for controlling the $B_d^0$ P-V channels. This global fit now combines CP asymmetries from $B_d^0 \to J/\psi K_S^0$, $B_d^0 \to J/\psi\pi^0$, $B_s^0 \to J/\psi K_S^0$, $B_d^0 \to J/\psi\rho^0$ and $B_s^0 \to J/\psi\phi$ together with the external input for $\gamma$ and $\epsilon$. It is important to note that by using $SU(3)$ symmetry we can assume that the penguin parameters from $B_s^0 \to J/\psi K_S^0$, $B_d^0 \to J/\psi K_S^0$ and $B_d^0 \to J/\psi\pi^0$ are equal to one another as shown in (2.72). The same reasoning is also used to assume that the penguin parameters from $B_s^0 \to J/\psi\phi$ and $B_d^0 \to J/\psi\rho^0$ are equal. Furthermore, it is also assumed that contributions from exchange and penguin annihilation topologies can be neglected.

From the global fit, we obtain for the P-V channels

$$a = 0.13^{+0.16}_{-0.10}, \qquad \theta = (173^{+34}_{-43})^\circ, \qquad \phi_d = (44.4^{+1.6}_{-1.5})^\circ, \quad (4.12)$$

and the values of $a$ and $\theta$ result in a phase shift

$$\Delta\phi_d = (-0.73^{+0.60}_{-0.91})^\circ. \quad (4.13)$$

For the V-V channels we obtain

$$a_V = 0.043^{+0.082}_{-0.037}, \qquad \theta_V = (306^{+48}_{-112})^\circ, \qquad \phi_s = (-5.0^{+1.6}_{-1.5})^\circ = -0.088^{+0.028}_{-0.027}, \quad (4.14)$$

and the values for $a_V$ and $\theta_V$ result in a phase shift

$$\Delta\phi_s = (0.14^{+0.54}_{-0.70})^\circ = 0.003^{+0.010}_{-0.012}. \quad (4.15)$$

The two-dimensional confidence regions for the combined fit to $\phi_d$ and $\phi_s$ are shown in Fig. 4.4 and Fig. 4.5. As mentioned before, including $B_s^0 \to J/\psi K_S^0$ to the P-V fit removed the ambiguous result for $a$ that was previously seen. The correlation between $a$ and $\phi_d$ is still present. For the V-V fits the results for $a_V$ and $\theta_V$ are unambiguous, but the fit does show a small region which would allow for a high value for $a_V$ which is disfavoured for the same reasons mentioned previously for $a$. Including this region

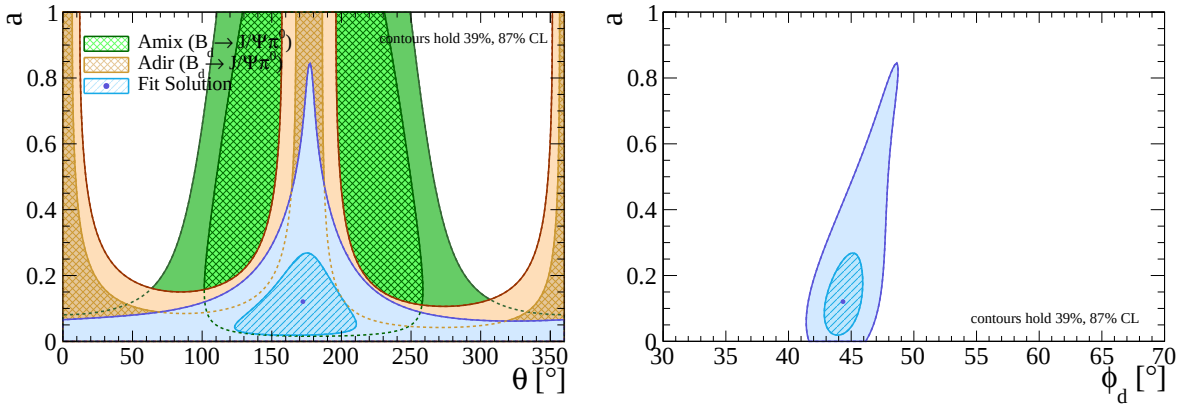


(a) (b)

Figure 4.4: Two-dimensional confidence regions for the combined fit to $B^0_d \to J/\psi K^0_S$, $B^0_d \to J/\psi\pi^0$ and $B^0_s \to J/\psi K^0_S$. (a) shows the fit to $a$ and $\theta$ and (b) shows the correlation between $a$ and $\phi_d$

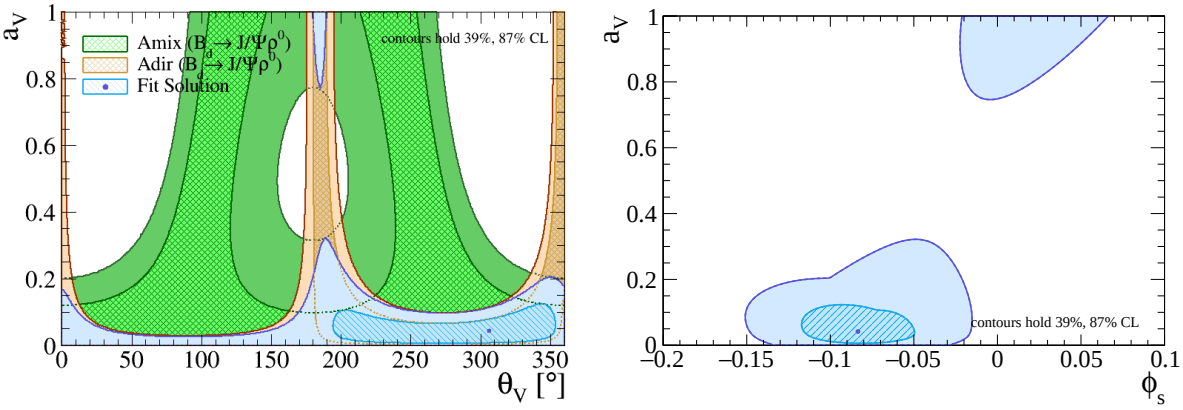


(a) (b)

Figure 4.5: Two-dimensional confidence regions for the combined fit to $B^0_d \to J/\psi\rho^0$ and $B^0_s \to J/\psi\phi$. (a) shows the fit to $a_V$ and $\theta_V$ and (b) shows the correlation between $a_V$ and $\phi_s$

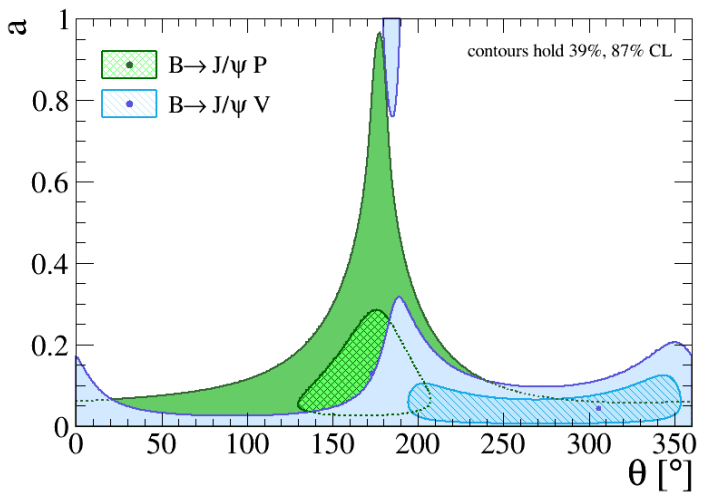


Figure 4.6: Comparison between the P-V and V-V mode penguin parameter fit solutions.

does again show a sizeable correlation between $a_V$ and $\phi_s$, once again highlighting the importance of controlling the penguin effects.

Now that we have the results for both the P-V and the V-V penguin parameters, it is worthwhile to visually highlight the fact that the P-V penguin parameters cannot be set to be equal to the V-V ones. Fig. 4.6 shows the combined fit regions for both the P-V and the V-V modes in one plot. It can be easily seen that the fit solutions do not agree with each other leading to the conclusion that $ae^{i\theta} \neq a_V e^{i\theta_V}$.

# Chapter 5

# Conclusion and outlook

Now that the theory, methods and results have been shown, it is time to draw conclusions and look at the possibilities this research could provide in the future. Let us begin by recalling the goals set out in the introduction. The initial goals were to determine the penguin parameters in neutral $B$ decays; To find the size of the penguin corrections in the weak mixing phases; And to obtain clean measurements of these mixing phases.

In order to make a fit to the penguin parameters and the mixing phases from experimental data we developed a new module that can be used within the GammaCombo framework. The end result of this is a global fit to all penguin parameters, and most importantly, the mixing phases. This effectively allowed us to bypass the second goal of this thesis. Since the size of the penguin corrections can still be insightful when trying to establish how the error on the mixing phases can be improved, they were calculated after the fact from the penguin parameters obtained from the fit. The final results for the mixing phases are

$$\phi_d = (44.4^{+1.6}_{-1.5})^\circ, \qquad \phi_s = (-5.0^{+1.6}_{-1.5})^\circ = -0.088^{+0.028}_{-0.027}, \tag{5.1}$$

with the corresponding phase shifts

$$\Delta\phi_s = (-0.75^{+0.61}_{-0.91})^\circ, \qquad \Delta\phi_s = (0.14^{+0.55}_{-0.71})^\circ = 0.003^{+0.010}_{-0.012}. \tag{5.2}$$

Looking back at the external inputs for $\phi_d$ and $\phi_s$ we can see that the result for $\phi_d$ matches the external input quite well[1]. For $\phi_s$ the difference is somewhat larger at $0.067 \pm 0.041$. Whilst this difference deviates from zero at 1.6 $\sigma$ the fitted value of $\phi_s$ is still in agreement with the external input. It is notable however that the error on $\phi_s$ coming from the external fit is already slightly larger than the value obtained here.

Whilst the external inputs provide a nice reference to compare the fit values against, it does not tell us anything about possible NP effects, which is one of the primary motivators for this research. In order to get a signal for NP we need to compare our fit value against the SM predictions for the mixing phases. The SM values are [35]

$$\phi_d^{SM} = (45.7 \pm 2.0)^\circ, \qquad \phi_s^{SM} = (-2.15 \pm 0.11)^\circ = -0.0376 \pm 0.0020. \tag{5.3}$$

Using these values and (1.1), $\phi^{NP}$ can be extracted, yielding

$$\phi_d^{NP} = (-1.3^{+2.6}_{-2.5})^\circ, \qquad \phi_s^{NP} = (-2.85^{+1.6}_{-1.5})^\circ = -0.050^{+0.028}_{-0.027}. \tag{5.4}$$

[1] the difference being $(-0.12 \pm 2.1)^\circ$

Here we see the same pattern emerge as with the external inputs above, the value for $\phi_d^{NP}$ does not show a significant deviation from zero at 0.5 $\sigma$, whilst the value for $\phi_s^{NP}$ deviates from zero at 1.8 $\sigma$. So at this point in time, we do not find a significant signal for NP in these mixing phases.

It is however worthwhile to explore how this picture might change in the future, considering also the expectation of more precise results from the LHC upgrade era and Belle II.

Assuming that the central values of the experimental input do not change, we can explore future scenarios by artificially reducing the error on these inputs. Beginning with a factor 2 improvement, the error on $\phi_d$ would become 0.78° and the error on $\phi_s$ 0.77°. In turn, this would improve the signal for NP to 0.6 and 3.5 $\sigma$ respectively. Going one step further with a factor 5 improvement, the error on $\phi_d$ becomes 0.31° and the error on $\phi_s$ 0.32°, leading to a NP signal of 0.64 and 8.3 (!) $\sigma$. The combined fit regions for these scenarios are shown in Fig. 5.1.

These future scenarios show that the combined fit approach explored in this thesis can lead to the discovery of NP in the future. As it stands now the precision on the SM prediction of $\phi_s$ is already sufficient to allow for NP to be found. More notably however, the SM prediction on $\phi_d$ already is and can quickly become the dominant contribution to error of the NP signal, so simply improving the experimental precision is not enough to discover NP in $B_d^0$ mixing.

The attentive reader might have noticed at this point that I have not made use of the observable $H$ discussed at the end of Chapter 2. Initially the plan was to make use of this observable to estimate the size of $SU(3)$ breaking in the amplitude ratio $|\mathcal{A}'/\mathcal{A}|$. In the final fit results however, it was clear that no $SU(3)$ breaking effects are observed at the current level of precision, requiring an order of magnitude improvement in order to detect any effect. Should this improvement be realized in the future, it will be important to take these effects into account in order to achieve the highest possible precision. The observable $H$ may in the future also be used as an additional constraint on the penguin parameters, since it only depends on $\mathcal{A}_{\mathrm{CP}}^{\mathrm{dir}}$. It therefore enables us to add channels for which only $\mathcal{A}_{\mathrm{CP}}^{\mathrm{dir}}$ is available. The only issue with this might be that $H$ is also sensitive to these $SU(3)$ breaking effects, so it should also be used carefully if more precise experimental input becomes available.

I would also like to highlight again the successful implementation of the GammaCombo fitting module. It allowed us to easily construct a single module with which the global fit could be made, as well as fits to individual decay channels. Besides being used for obtaining the mixing phases, the same module has also been used for obtaining effective Wilson coefficients for $B_s^0 \to J/\psi K_S^0$ and $B_d^0 \to J/\psi K_S^0$ which are reported in [35]. The motivation for utilizing GammaCombo for making this fit was to enable other groups to implement it in order to control these penguin effects, as these are currently often neglected in literature. Since the results obtained here show that controlling the penguin contributions is vital for finding signals of NP, I hope that this will encourage other groups to start using the formalism presented here to improve their own results.

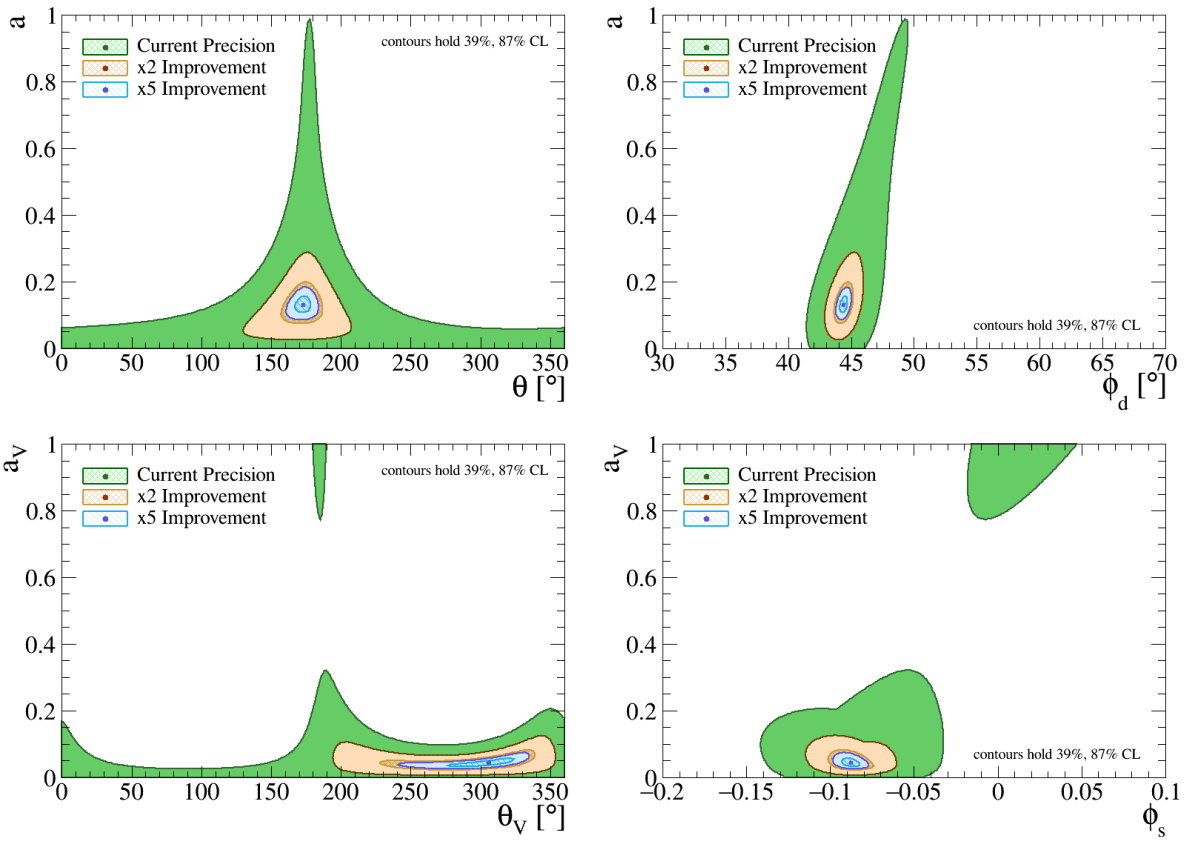


Figure 5.1: Combined fit regions for the global fit to the penguin parameters and mixing phases. Showing the current fit regions combined with future scenarios with a factor 2 and 5 improvement of the precision of experimental input measurements.

# Acknowledgements

As a final note, I want to thank several people for their help in my thesis. Beginning with my daily supervisor, Robert Fleischer, for inviting me to do this project with him at the Nikhef institute.
I also thank Kristof de Bruyn for his help with developing the GammaCombo module and for cleaning up the plots showing the fit results and future scenarios, as well as Eleftheria Malami for answering questions that came up during this project.
Then I want to thank all three of them again, for allowing me the opportunity to collaborate with them in writing and (hopefully) publishing a paper which includes the results shown in this thesis, it has been a wonderful experience.
A final thanks also to my fellow master students at the Nikhef Theory group, which made the time spent there all the more enjoyable.

# Bibliography


[1] Mary K. Gaillard, Paul D. Grannis, and Frank J. Sciulli. "The Standard model of particle physics". In: *Rev. Mod. Phys.* 71 (1999), S96–S111. DOI: 10.1103/RevModPhys.71.S96. arXiv: hep-ph/9812285.

[2] Georges Aad et al. "Observation of a new particle in the search for the Standard Model Higgs boson with the ATLAS detector at the LHC". In: *Phys. Lett. B* 716 (2012), pp. 1–29. DOI: 10.1016/j.physletb.2012.08.020. arXiv: 1207.7214 [hep-ex].

[3] Serguei Chatrchyan et al. "Observation of a New Boson at a Mass of 125 GeV with the CMS Experiment at the LHC". In: *Phys. Lett. B* 716 (2012), pp. 30–61. DOI: 10.1016/j.physletb.2012.08.021. arXiv: 1207.7235 [hep-ex].

[4] J. H. Christenson, J. W. Cronin, V. L. Fitch, and R. Turlay. "Evidence for the $2\pi$ Decay of the $K_2^0$ Meson". In: *Phys. Rev. Lett.* 13 (4 July 1964), pp. 138–140. DOI: 10.1103/PhysRevLett.13.138. URL: https://link.aps.org/doi/10.1103/PhysRevLett.13.138.

[5] A.D. Sakharov. "Violation of CP Invariance, C asymmetry, and baryon asymmetry of the universe". In: *Sov. Phys. Usp.* 34.5 (1991), pp. 392–393. DOI: 10.1070/PU1991v034n05ABEH002497.

[6] Nicola Cabibbo. "Unitary Symmetry and Leptonic Decays". In: *Phys. Rev. Lett.* 10 (12 June 1963), pp. 531–533. DOI: 10.1103/PhysRevLett.10.531. URL: https://link.aps.org/doi/10.1103/PhysRevLett.10.531.

[7] Makoto Kobayashi and Toshihide Maskawa. "CP-Violation in the Renormalizable Theory of Weak Interaction". In: *Progress of Theoretical Physics* 49.2 (Feb. 1973), pp. 652–657. ISSN: 0033-068X. DOI: 10.1143/PTP.49.652. eprint: https://academic.oup.com/ptp/article-pdf/49/2/652/5257692/49-2-652.pdf. URL: https://doi.org/10.1143/PTP.49.652.

[8] S. W. Herb et al. "Observation of a Dimuon Resonance at 9.5 GeV in 400-GeV Proton-Nucleus Collisions". In: *Phys. Rev. Lett.* 39 (5 Aug. 1977), pp. 252–255. DOI: 10.1103/PhysRevLett.39.252. URL: https://link.aps.org/doi/10.1103/PhysRevLett.39.252.

[9] F. Abe et al. "Observation of top quark production in $\bar{p}p$ collisions". In: *Phys. Rev. Lett.* 74 (1995), pp. 2626–2631. DOI: 10.1103/PhysRevLett.74.2626. arXiv: hep-ex/9503002.

[10] Kazuo Abe et al. "An Improved measurement of mixing induced CP violation in the neutral B meson system". In: *Phys. Rev. D* 66 (2002), p. 071102. DOI: 10.1103/PhysRevD.66.071102. arXiv: hep-ex/0208025.

[11] Bernard Aubert et al. "Measurement of the CP-violating asymmetry amplitude $\sin 2\beta$". In: *Phys. Rev. Lett.* 89 (2002), p. 201802. DOI: 10.1103/PhysRevLett.89.201802. arXiv: hep-ex/0207042.

[12] Nobel Prize Committee. *The Nobel Prize in Physics 2008*. URL: https://www.nobelprize.org/prizes/physics/2008/summary/. (accessed: 05-08-2020).

[13] Mikhail A. Shifman. "Foreword to ITEP lectures in particle physics". In: *ITEP Lectures in Particle Physics and Field Theory* (Oct. 1995), pp. v–xi. arXiv: hep-ph/9510397.

[14] Robert Fleischer. "Extracting $\gamma$ from $B(s/d) \to J/\psi K_S$ and $B(d/s) \to D^+(d/s)D^-(d/s)$". In: *Eur. Phys. J. C* 10 (1999), pp. 299–306. DOI: 10.1007/s100529900099. arXiv: hep-ph/9903455.

[15] Robert Fleischer. "Extracting CKM phases from angular distributions of $B_{d,s}$ decays into admixtures of CP eigenstates". In: *Phys. Rev. D* 60 (1999), p. 073008. DOI: 10.1103/PhysRevD.60.073008. arXiv: hep-ph/9903540.

[16] Sven Faller, Martin Jung, Robert Fleischer, and Thomas Mannel. "The Golden Modes B0 —> J/psi K(S,L) in the Era of Precision Flavour Physics". In: *Phys. Rev. D* 79 (2009), p. 014030. DOI: 10.1103/PhysRevD.79.014030. arXiv: 0809.0842 [hep-ph].

[17] Kristof De Bruyn, Robert Fleischer, and Patrick Koppenburg. "Extracting gamma and Penguin Topologies through CP Violation in B_sˆ0 -> J/psi K_S". In: *Eur. Phys. J. C* 70 (2010), pp. 1025–1035. DOI: 10.1140/epjc/s10052-010-1495-z. arXiv: 1010.0089 [hep-ph].

[18] Kristof De Bruyn and Robert Fleischer. "A Roadmap to Control Penguin Effects in $B_d^0 \to J/\psi K_S^0$ and $B_s^0 \to J/\psi\phi$". In: *JHEP* 03 (2015), p. 145. DOI: 10.1007/JHEP03(2015)145. arXiv: 1412.6834 [hep-ph].

[19] LHCb. *GammaCombo*. URL: https://gammacombo.github.io. (accessed: 30-07-2020).

[20] F. Englert and R. Brout. "Broken Symmetry and the Mass of Gauge Vector Mesons". In: *Phys. Rev. Lett.* 13 (1964). Ed. by J.C. Taylor, pp. 321–323. DOI: 10.1103/PhysRevLett.13.321.

[21] Peter W. Higgs. "Broken Symmetries and the Masses of Gauge Bosons". In: *Phys. Rev. Lett.* 13 (1964). Ed. by J.C. Taylor, pp. 508–509. DOI: 10.1103/PhysRevLett.13.508.

[22] G.S. Guralnik, C.R. Hagen, and T.W.B. Kibble. "Global Conservation Laws and Massless Particles". In: *Phys. Rev. Lett.* 13 (1964). Ed. by J.C. Taylor, pp. 585–587. DOI: 10.1103/PhysRevLett.13.585.

[23] P.A. Zyla et al. "Review of Particle Physics". In: *PTEP* 2020.8 (2020), p. 083C01. DOI: 10.1093/ptep/ptaa104.

[24] Particle Data Group. *Particle Data Group - 2020 Review*. URL: https://pdg.lbl.gov. (accessed: 27-07-2020).

[25] Lincoln Wolfenstein. "Parametrization of the Kobayashi-Maskawa Matrix". In: *Phys. Rev. Lett.* 51 (1983), p. 1945. DOI: 10.1103/PhysRevLett.51.1945.

[26] Andrzej J. Buras, Markus E. Lautenbacher, and Gaby Ostermaier. "Waiting for the top quark mass, K+ —> pi+ neutrino anti-neutrino, B(s)0 - anti-B(s)0 mixing and CP asymmetries in B decays". In: *Phys. Rev. D* 50 (1994), pp. 3433–3446. DOI: 10.1103/PhysRevD.50.3433. arXiv: hep-ph/9403384.

[27] Alexandra Martin Sanchez. "Measurement of the gamma angle from tree decays at the LHCb experiment". In: *EPJ Web Conf.* 28.arXiv:1201.4736 (Jan. 2012). Comments: Presented at the 2011 Hadron Collider Physics symposium (HCP-2011), Paris, France, November 14-18 2011, 3 pages, 9 figures, 12030. 3 p. DOI: 10.1051/epjconf/20122812030. URL: https://cds.cern.ch/record/1418719.

[28] CKMfitter collaboration. *CKMfitter*. URL: ckmfitter.in2p3.fr. For the latest fit results see also http://ckmfitter.in2p3.fr/www/results/plots_summer19/num/ckmEval_results_summer19.html. (accessed: 14-08-2020).

[29] UTfit collaboration. *UTfit WebHome*. URL: https://utfitorg/UTfit/. (accessed: 01-08-2020).

[30] Andrzej J. Buras. "Weak Hamiltonian, CP violation and rare decays". In: *Les Houches Summer School in Theoretical Physics, Session 68: Probing the Standard Model of Particle Interactions*. June 1998, pp. 281–539. arXiv: hep-ph/9806471.

[31] Robert Fleischer. "CP violation in the B system and relations to K —> pi nu anti-nu decays". In: *Phys. Rept.* 370 (2002), pp. 537–680. DOI: 10.1016/S0370-1573(02)00274-0. arXiv: hep-ph/0207108.

[32] Yasmine Sara Amhis et al. "Averages of $b$-hadron, $c$-hadron, and $\tau$-lepton properties as of 2018". In: (Sept. 2019). arXiv: 1909.12524 [hep-ex].

[33] R Aaij et al. "Measurement of the CKM angle $\gamma$ from a combination of $B^{\pm} \to Dh^{\pm}$ analyses". In: *Phys. Lett. B* 726 (2013), pp. 151–163. DOI: 10.1016/j.physletb.2013.08.020. arXiv: 1305.2050 [hep-ex].

[34] Matthew William Kenzie and Mark Peter Whitehead. "Update of the LHCb combination of the CKM angle $\gamma$". In: (May 2018).

[35] Marten Z. Barel, Kristof De Bruyn, Robert Fleischer, and Eleftheria Malami. "In Pursuit of New Physics with $B_d^0 \to J/\psi K^0$ and $B_s^0 \to J/\psi\phi$ Decays at the High-Precision Frontier". In: (Oct. 2020). arXiv: 2010.14423 [hep-ph].

[36] Roel Aaij et al. "Measurement of the time-dependent CP asymmetries in $B_s^0 \to J/\psi K_S^0$". In: *JHEP* 06 (2015), p. 131. DOI: 10.1007/JHEP06(2015)131. arXiv: 1503.07055 [hep-ex].

[37] Roel Aaij et al. "Measurement of the CP-violating phase $\beta$ in $B^0 \to J/\psi\pi^+\pi^-$ decays and limits on penguin effects". In: *Phys. Lett. B* 742 (2015), pp. 38–49. DOI: 10.1016/j.physletb.2015.01.008. arXiv: 1411.1634 [hep-ex].